Cluster Expansion Reactions of Group 6 Metallaboranes. Syntheses, Crystal Structures, and Spectroscopic Characterizations of $(Cp^*Cr)_2B_5H_9$, $(Cp^*Cr)_2B_4H_8Fe(CO)_3$, $(Cp^*Cr)_2B_4H_7Co(CO)_3$, and $(Cp^*Mo)_2B_5H_9Fe(CO)_3$

Simon Aldridge, Hisako Hashimoto, Kazumori Kawamura, Maoyu Shang, and Thomas P. Fehlner*

Department of Chemistry and Biochemistry, University of Notre Dame, Notre Dame, Indiana 46556

Received October 1, 1997

The targeted high-yield syntheses of a number of new clusters by the controlled addition of BH, $Fe(CO)_3$, or $Co(CO)_3$ fragments to dinuclear group 6 metallaboranes are reported. The reaction of the chromaborane, $(Cp^*Cr)_2B_4H_8$ (**1**), $Cp^* = \eta^5$-C_5Me_5, with $BHCl_2{\cdot}SMe_2$ results in a cluster expansion reaction giving the green-brown diamagnetic species $(Cp^*Cr)_2B_5H_9$ (**2**) in 43% yield. The six skeletal electron pair (sep) cluster has a structure based on a trigonal bipyramidal Cr_2B_3 unit with adjacent Cr_2B faces capped by BH_3 fragments. Reaction of **1** with the dinuclear metal carbonyls $Fe_2(CO)_9$ and $Co_2(CO)_8$ leads to the isolation of the mixed-metal metallaboranes $(Cp^*Cr)_2B_4H_8Fe(CO)_3$ (**3**) and $(Cp^*Cr)_2B_4H_7Co(CO)_3$ (**4**) in yields of 76 and 87%, respectively. **3** and **4** can also be viewed as six-sep bicapped trigonal bipyramidal clusters with the metal carbonyl occupying one of the capping positions. Alternatively, they can be viewed as complexes between $M(CO)_3$ transition metal fragments (M = Fe, Co) and the four-electron $(Cp^*Cr)_2B_4H_8$ (M = Fe) or three-electron $(Cp^*Cr)_2B_4H_7$ (M = Co) ligands. In this way, by forming two M−Cr bonds and utilizing either one (M = Co) or two (M = Fe) BH→M donor−acceptor bonds, each metal attains an 18-electron configuration. At elevated temperatures (ca. 80 °C), **3** is fluxional, with the $Fe(CO)_3$ fragment "swinging" between equivalent pairs of BH_2 donor groups. Reaction of the molybdaborane $(Cp^*Mo)_2B_5H_9$ (**5**) with $Fe_2(CO)_9$ gives the orange mixed-metal cluster $(Cp^*Mo)_2B_5H_9Fe(CO)_3$ (**6**) in 48% yield. **6** has a bicapped octahedral geometry with the $Fe(CO)_3$ fragment occupying one of the high-connectivity cluster vertexes, rather than a capping position. That **5** undergoes the expected geometric changes (bicapped trigonal bipyramid → bicapped octahedron) on addition of the two-electron $Fe(CO)_3$ fragment (giving **6**) contrasts with the minimal structural perturbation on addition of the same fragment to **1** (yielding **3**). This in turn provides further evidence for the description of **1** as an "electronically unsaturated" cluster.

Introduction

Controlled high-yield synthesis of specifically targeted cluster compounds is often difficult to achieve. Within the realms of metallaborane chemistry, two complementary approaches to the buildup of clusters from transition metal complexes have received much attention,[1−4] viz. (i) condensation reactions involving monoboron precursors and (ii) insertion or fragmentation reactions involving "pre-assembled" borane fragments. In each case, the accessibility under the conditions employed of many minima on the reaction pathway often leads to the formation of a range of products with varying M:B ratios, each produced in low yield.[5−11]

The recent synthesis of electronically unsaturated metallaboranes—that is those which are formally electron deficient with respect to the number of skeletal pairs required to sustain the observed molecular geometry—exemplified by $(Cp^*Cr)_2B_4H_8$ (**1**),[12] $(Cp^*MoCl)_2B_3H_7$,[13] and $Cp^*TaCl_2B_4H_8$ ($Cp^* = \eta^5$-C_5Me_5)[14] offers an attractive alternative route to a variety of larger clusters. This synthetic utility is derived from the propensity of the unsaturated cluster to react with fragments which can readily donate further electrons to the cluster framework. Hence, reaction of **1** with sources of BH and $M(CO)_3$ fragments (M = Fe, Co) brings about the synthesis of the three novel metallaboranes $(Cp^*Cr)_2B_5H_9$ (**2**), $(Cp^*Cr)_2B_4H_8Fe(CO)_3$ (**3**),[15] and $(Cp^*Cr)_2B_4H_7Co(CO)_3$ (**4**) in good yield. The clusters **2**−**4** have the same skeletal electron count, and comparison of their

(1) Kennedy, J. D. *Prog. Inorg. Chem.* **1984**, *32*, 519.
(2) Kennedy, J. D. *Prog. Inorg. Chem.* **1986**, *34*, 211.
(3) Housecroft, C. E.; Fehlner, T. P. *Adv. Organomet. Chem.* **1982**, *21*, 57.
(4) Grimes, R. N. In *Metal Interactions with Boron Clusters*; Grimes, R. N., Ed.; Plenum: New York, 1982; p 269.
(5) Vites, J. C.; Housecroft, C. E.; Eigenbrot, C.; Buhl, M. L.; Long, G. J.; Fehlner, T. P. *J. Am. Chem. Soc.* **1986**, *108*, 3304.
(6) Grebenik, P. D.; Green, M. L. H.; Kelland, M. A.; Leach, J. B.; Mountford, P.; Stringer, G.; Walker, N. M.; Wong, L. L. *J. Chem. Soc., Chem. Commun.* **1988**, 799.
(7) Coffy, T. J.; Medford, G.; Plotkin, J.; Long, G. J.; Shore, S. G. *Organometallics* **1989**, *8*, 2404.
(8) Grebenik, P. D.; Green, M. L. H.; Leach, J. B.; Walker, N. M. *J. Organomet. Chem.* **1988**, *345*, C13.
(9) Grebenik, P. D.; Leach, J. B.; Kelland, M. A.; Green, M. L. H.; Mountford, P. *J. Chem. Soc., Chem. Commun.* **1989**, 1397.
(10) Ting, C.; Messerle, L. *J. Am. Chem. Soc.* **1989**, *111*, 3449.
(11) Meng, X.; Bandyopadhyay, A. K.; Fehlner, T. P.; Grevels, F.-W. *J. Organomet. Chem.* **1990**, *394*, 15.
(12) Deck, K. J.; Nishihara, Y.; Shang, M.; Fehlner, T. P. *J. Am. Chem. Soc.* **1995**, *117*, 10292.
(13) Aldridge, S.; Shang, M.; Fehlner, T. P. *J. Am. Chem. Soc.* **1997**, *119*, 11120.
(14) Aldridge, S.; Hashimoto, H.; Shang, M.; Fehlner, T. P. *J. Chem. Soc., Chem. Commun.* **1998**, 207.
(15) Hashimoto, H.; Shang, M.; Fehlner, T. P. *J. Am. Chem. Soc.* **1996**, *118*, 8164.

S0020-1669(97)01251-2 CCC: $15.00
Published on Web 02/19/1998

Table 1. ^{11}B NMR of the Metallaboranes **2**−**4** and **6**[a]

	2	**3**		**4**	**6**
temp (°C)	22	−20	80	22	22
B−M	91.5 B(2), B(4) 86.2 B(3)	129.5 105.8	117.5 B(2), B(3)	121.7 B(2) 113.9 B(3)	90.4 B(2), B(3) −0.4 B(4)
B−H−M	25.0 B(1), B(5)	46.0 4.1	27.3 B(1), B(4)	57.5 B(1) 36.6 B(4)	41.4 B(1) 29.7 B(5)

[a] The numbering scheme for each molecule was taken from the appropriate figure.

Table 2. ^{1}H NMR of the Metallaboranes **2**−**4** and **6**[a]

	2	**3**		**4**	**6**
temp (°C)	22	−20	80	22	22
B−*H*−M	−6.2 (4)	−16.2 (2)[b] −8.0 (2)[c]	−11.9 (4)	−13.8 (1)[b] −5.6 (2)[c]	−15.5 [2, B(1)−Mo] −13.1 [2, B(5)−Mo]
B−*H*	3.2 (1) 4.6 (2) 6.7 (2)	≈2 (2) ≈7 (2)	≈2 (2) ≈7 (2)	≈7 (2) ≈2.5 (2)	0.9 [1, B(4)−H] 3.9 [2, accid overlap of B(1)−H, B(5)−H] 8.0 [2, B(2,3)−H]

[a] Relative intensities are given in parentheses (or brackets, in last column). [b] CrMB (M = Fe or Co) face-bridging. [c] Cr−B edge-bridging.

geometric and electronic structures offers insight into the role of the BH and $M(CO)_3$ fragments in influencing cluster geometry. Whereas **3** and **4** can be described in terms of a coordination complex between a metal carbonyl fragment and a four- or three-electron metallaborane ligand, **2** fits more easily into the category of a conventional metallaborane cluster.

Extension of this approach to the molybdaborane $(Cp^*Mo)_2B_5H_9$ (**5**) and synthesis of the mixed iron/molybdenum cluster $(Cp^*Mo)_2B_5H_9Fe(CO)_3$ (**6**) allows comparison of structures and reactivities for the chromium and molybdenum systems. In addition, the geometric changes occurring in the Mo_2B_5 cluster framework on addition of the $Fe(CO)_3$ fragment (to give **6**) contrast starkly with the minimal structural changes occurring in the analogous Cr_2B_4 unit on going from **1** to **3**.[15] These contrasting results provide further indirect evidence for the electronic unsaturation inherent in cluster **1**.[12,16] Finally, the electronic factors underlying the apparent differences in reactivity between M_2B_4 and M_2B_5 systems and between chromium and molybdenum clusters have been probed by Fenske−Hall methods.[17,18] Interestingly, these reveal larger HOMO/LUMO gaps in the case of molybdenum (attributed to better M−M and M−B overlap for Mo vs Cr) and for the B_5 clusters (principally due to an extra bonding interaction between a M−M δ^* orbital and the p_z orbital of the extra unique boron atom).

Experimental Section

General Procedures. All manipulations were carried out under a nitrogen or argon atmosphere using standard Schlenk-line or drybox techniques. Solvents were predried over 4-Å molecular sieves (tetrahydrofuran) or KOH (hexanes, toluene) and purged with nitrogen prior to distillation. Tetrahydrofuran (thf), toluene, and hexanes were all distilled from sodium benzophenone ketal. The starting material for the chromaboranes, $(Cp^*CrCl)_2$, was prepared according to published procedures,[19] with several modifications designed to minimize decomposition due to reaction with air or moisture.[12] $(Cp^*Cr)_2B_4H_8$ (**1**) was prepared from $(Cp^*CrCl)_2$ according to published procedures.[12] Starting materials for the molybdaboranes, Cp^*MoCl_4 or $(Cp^*MoCl_2)_2$, were prepared according to the methods of King,[20] Schrock,[21] and Green.[22] The BH_3·thf solution and $BHCl_2$·SMe_2 (Aldrich) were used as received without further purification, as were samples of $Fe_2(CO)_9$ (Aldrich) and $Co_2(CO)_8$ (Strem).

Table 3. Selected IR Bands of the Metallaboranes **2**−**4** and **6** (cm^{-1})[a]

	2	**3**	**4**	**6**
ν(CO)	*b*	1978 vs 1916 vs 1905 vs	2019 s 1974 m 1908 w	1994 vs 1947 s 1934 s
$\nu(BH_t)$	2476 s 2452 s	2494 m 2484 m 2466 w, sh 2446 w	2487 m 2472 m, sh 2442 w	2479 m 2467 m, sh 2423 w

[a] **2**, **3**, and **6** in the form of KBr disks; **4** as a hexane solution. [b] Not applicable.

NMR spectra were measured on a Varian-300 or Varian-500 FT-NMR spectrometer. Residual protons of solvent were used for reference for ^{1}H NMR (δ, ppm: benzene, 7.15; dichloromethane, 5.32; toluene, 2.09). For ^{13}C NMR, solvent signals were also used as the chemical shift reference, while a sealed tube containing $[(NEt_4)(B_3H_8)]$ (δ_B −29.7 ppm) was used as the external reference for ^{11}B NMR. Infrared spectra were measured on a Nicolet 205 FT-IR spectrometer. Mass spectra were measured on a JEOL JMS-AX 505HA mass spectrometer using the EI ionization mode. Perfluorokerosene was used as the standard for high-resolution EI mass spectra.

Synthesis of $(Cp^*Cr)_2B_5H_9$ (2). To a toluene solution containing 313 mg (0.74 mmol) of **1** was added a 3-fold excess of $BHCl_2$·SMe_2 at room temperature and the reaction mixture warmed to 55 °C. After a reaction time of 72 h, volatiles were removed in vacuo and hexane extraction followed by filtration through predried Celite was carried out to yield the crude product [140 mg, 0.32 mmol of $(Cp^*Cr)_2B_5H_9$ (**2**) or 43% based on the amount of **1** taken]. Concentration of a hexane solution and cooling to −40 °C led to the growth of brown platelike crystals over a 24 h period. **2** can also be prepared by the reaction of **1** with BH_3·thf in toluene at 55 °C, although the reaction is much slower than that with $BHCl_2$·SMe_2, being only 70% complete after 3 weeks (as judged by integration of ^{11}B NMR signals). **2** is slightly air-sensitive in the solid phase and much more so in solution and has been characterized by measurement of its ^{1}H, ^{11}B, and ^{13}C NMR spectra, solid-phase IR spectrum, and EI mass spectrum[23] and by single-crystal X-ray diffraction. Selected spectroscopic data are given in Tables 1−3.

(16) Fehlner, T. P. *J. Organomet. Chem.*, in press.
(17) Fenske, R. F. *Pure Appl. Chem.* **1988**, *27*, 61.
(18) Hall, M. B.; Fenske, R. F. *Inorg. Chem.* **1972**, *11*, 768.
(19) Heintz, R. A.; Haggerty, B. S.; Wan, H.; Rheingold, R. L.; Theopold, K. H. *Angew. Chem., Int. Ed. Engl.* **1992**, *31*, 1077.
(20) King, R. B.; Bisnette, M. B. *J. Organomet. Chem.* **1967**, *8*, 287.
(21) Murray, R. C.; Blum, L.; Liu, A. H.; Schrock, R. R. *Organometallics* **1985**, *4*, 953.
(22) Green, M. L. H.; Hubert, J. D.; Mountford, P. *J. Chem. Soc., Dalton Trans.* **1990**, 3793.
(23) Aldridge, S.; Fehlner, T. P.; Shang, M. *J. Am. Chem. Soc.* **1997**, *119*, 2339.

Table 4. Crystal Data and Structure Refinement Details for Compounds **2**−**4** and **6**

	2	**3**	**4**	**6**
formula weight	437.56	565.62	567.70	665.32
crystal system	tetragonal	monoclinic	orthorhombic	orthorhombic
space group	$P4_2/n$	$P2_1/n$	*Pbcn*	*Fdd2*
a (Å)	23.711(2)	8.4967(6)	27.868(3)	24.679(7)
b (Å)	23.711(2)	20.730(2)	11.373(3)	25.126(2)
c (Å)	8.4380(4)	15.2848(10)	16.884(2)	17.958(2)
β (deg)		90.277(6)		
V (Å^3)	4744.0(7)	2685.8(4)	5352(2)	11135(3)
Z	8	4	8	16
ρ_{calcd} (g cm^{-3})	1.225	1.399	1.409	1.587
temp (K)	293(2)	293(2)	293(2)	293(2)
wavelength (Å)	0.710 73	0.710 73	0.710 73	0.710 73
abs coeff (cm^{-1})	9.19	13.50	14.32	14.24
crystal size (mm)	0.50 × 0.12 × 0.10	0.48 × 0.05 × 0.03	0.32 × 0.20 × 0.18	0.45 × 0.13 × 0.10
θ range (deg)	2.43−28.28	2.38−22.50	2.28−24.98	2.31−25.00
index ranges	$-30 \le h \le 28$ $-30 \le k \le 18$ $-10 \le l \le 6$	$-9 \le h \le 9$ $-22 \le k \le 0$ $-16 \le l \le 0$	$0 \le h \le 33$ $0 \le k \le 13$ $0 \le l \le 20$	$0 \le h \le 29$ $0 \le k \le 29$ $0 \le l \le 21$ $-29 \le h \le 0$ $-29 \le k \le 0$ $-21 \le l \le 0$
no. of reflns collected	29 246	3651	4692	5060
no. of independent reflns	5503 (R_{int} = 0.0788)	3502 (R_{int} = 0.0346)	4692	4890 (R_{int} = 0.0181)
no. of obsd reflns[a]	3724	2636	3021	4718
refinement method	full-matrix on F^2	full-matrix on F^2	full-matrix on F^2	full-matrix on F^2
data/restraints/parameters	5503/2/280	3502/0/330	4692/10/329	4890/9/336
goodness of fit on F^2	1.103	1.086	1.141	1.168
final *R* indices [$I > 2\sigma(I)$]	R1 = 0.0652 wR2 = 0.1484	R1 = 0.0508 wR2 = 0.1073	R1 = 0.0703 wR2 = 0.1404	R1 = 0.0390 wR2 = 0.0994
R indices (all data)[b]	R1 = 0.1046 wR2 = 0.1680	R1 = 0.0755 wR2 = 0.1254	R1 = 0.1241 wR2 = 0.1842	R1 = 0.0406 wR2 = 0.1009
largest diff peak and hole (e Å^{-3})	0.349 and −0.383	0.373 and −0.469	0.457 and −0.586	1.045 and −0.585

[a] $[I > 2\sigma(I)]$. [b] wR2 = $\{[\sum w(F_c^2 - F_o^2)^2]/[\sum w(F_o^2)^2]\}^{1/2}$.

Synthesis of $(Cp^*Cr)_2B_4H_8Fe(CO)_3$ (3). A solution of **1** (100 mg, 0.24 mmol) in toluene was added to $Fe_2(CO)_9$ (172 mg, 0.473 mmol) at room temperature and the reaction mixture warmed to 50 °C. After 72 h, volatiles were removed in vacuo and the resulting brown residue was extracted with hexane. Filtration through predried Celite yielded crude $(Cp^*Cr)_2B_4H_8Fe(CO)_3$ (**3**) (101 mg, 0.178 mmol, or 76% based on the amount of **1** taken); recrystallization from a toluene/hexane mixture gave a much purer product in the form of dark brown acicular crystals. **3** has been characterized by measurement of its ^{1}H, ^{11}B, and ^{13}C NMR spectra, solid-phase IR spectrum, and EI mass spectrum[15] and by single-crystal X-ray diffraction and is sufficiently stable in air that data collection could be accomplished simply by mounting the crystal on a glass fiber. Selected spectroscopic data are given in Tables 1−3.

Synthesis of $(Cp^*Cr)_2B_4H_7Co(CO)_3$ (4). A solution of **1** (200 mg, 0.47 mmol) in toluene was added to $Co_2(CO)_8$ (177 mg, 0.517 mmol) at −40 °C and the reaction mixture warmed to room temperature. After 22 h, the reaction mixture was filtered through predried Celite and volatiles were removed in vacuo, yielding crude $(Cp^*Cr)_2B_4H_7Co(CO)_3$ (**4**) (232 mg, 0.409 mmol, or 87% based on the amount of **1** taken) as an oily brown solid. A pure crystalline sample [free from traces of the coproduct $Co_4(CO)_{12}$] can be obtained by repeated recrystallization from hexane (in which the cobalt carbonyl is less soluble). Dark brown platelike crystals suitable for X-ray diffraction were then be grown by cooling a concentrated hexane solution to −40 °C. **4** has been characterized by ^{1}H, ^{11}B, and ^{13}C NMR, solution-phase IR (hexane), and EI mass spectrometry and by single-crystal X-ray diffraction. MS-(EI): P^+ *m*/*z* 568, 2 Cr and 4 B atoms; fragment peaks corresponding to sequential loss of 3 CO. *m*/*z*: calcd for weighted average of $^{12}C_{23}{}^1H_{37}{}^{11}B_4Co^{52}Cr_2{}^{16}O_3$, $^{12}C_{23}{}^1H_{37}{}^{10}B^{11}B_3Co^{52}Cr^{53}Cr^{16}O_3$, and $^{12}C_{22}$-$^{13}C^1H_{37}{}^{10}B^{11}B_3Co^{52}Cr_2{}^{16}O_3$ multiplet, 568.1279; obsd, 568.1255. IR (KBr, cm^{-1}): 2962 m, 2923 w, 2915 w, 2873 vw, sh, ν(C−H); 2487 m, 2472 m, sh, 2442 w, ν(B−H$_t$); 2019 s, 1974 m, 1908 w, ν(C−O). ^{13}C{^{1}H} NMR ([$^2H_6$]benzene, 295 K): δ 109.6 [C_5Me_5], δ 12.5 [$C_5\mathit{Me}_5$]. Further spectroscopic data are given in Tables 1−3.

Synthesis of $(Cp^*Mo)_2B_5H_9$ (5). Although the synthesis of $(C_5H_4MeMo)_2B_5H_9$ in 0.75−1.5% yield by the reaction of $C_5H_4MeMoCl_4$ with $LiBH_4$ in diethyl ether has previously been reported,[24] $(Cp^*Mo)_2B_5H_9$ (**5**) is most conveniently prepared by the reaction of either Cp^*MoCl_4, $(Cp^*MoCl_2)_2$, or "Cp^*MoCl" with BH_3·thf.[23] Reaction of Cp^*MoCl_4 with a 7-fold excess of BH_3·thf in toluene at 45 °C over a period of 120 h yields a mixture of **5** and the Mo(III) metallaborane $(Cp^*MoCl)_2B_4H_{10}$,[23] from which **5** is easily separated by extraction with hexane. Concentration of a hexane solution followed by cooling to −40 °C allows orange crystals of **5** to be isolated in yields of 30−40% based on the amount of Cp^*MoCl_4 used. Characterization of **5** was achieved by comparison of the measured NMR spectra with those reported for $(C_5H_4MeMo)_2B_5H_9$ (listed in parentheses).[24] ^{11}B NMR (hexane, 21 °C): δ 62.9 [lopsided doublet−accidental overlap of two signals, 3B] (δ 61.6, 2B, and 59.7, 1B), δ 25.8 [m, 2B] (27.8, 2B). ^{1}H NMR (toluene, 21 °C): δ −6.99 [pcq, 4H] (−7.01, 4H), δ 1.92 [s, 30H] (−), δ 3.85 [br, 1H] (3.94, 1H), 5.37 [br, 2H] (5.53, 2H), 6.22 [b, 2H], (6.34, 2H).

Synthesis of $(Cp^*Mo)_2B_5H_9Fe(CO)_3$ (6). A solution of **5** (139 mg, 0.26 mmol) in toluene was reacted with $Fe_2(CO)_9$ (145 mg, 0.4 mmol) at room temperature for 16 h. The initially orange solution became green, and the ^{11}B NMR spectrum measured at this point indicated the presence of four new signals (subsequently to be attributed to **6**) together with resonances due to unreacted **5**. Heating the reaction mixture to 45 °C failed to bring about further conversion so the solution was added to a further 400 mg (1.1 mmol) of $Fe_2(CO)_9$ and the reaction mixture heated for a further 48 h. At this point, conversion of **5** to **6** was judged to be complete by ^{11}B NMR and volatiles were removed in vacuo. Extraction with hexane yielded an orange solution and an insoluble green solid [which was shown by its IR spectrum to be $Fe_3(CO)_{12}$[25]]. Concentration of the orange solution and cooling to −10 °C yielded orange crystals of **6** (83 mg, 0.12 mmol, or 48% based on the amount

(24) Bullick, H. J.; Grebenik, P. D.; Green, M. L. H.; Hughes, A. K.; Leach, J. B.; McGowan, P. C. *J. Chem. Soc., Dalton Trans.* **1995**, 67.
(25) Poliakoff, M. *J. Chem. Soc. A* **1971**, 654.

of **5** taken). **6** is stable in air in both solid and solution phases and has been characterized by ^{1}H and ^{11}B NMR (including selective decoupling experiments), solid-state IR, and EI mass spectrometry and by single-crystal X-ray diffraction. MS(EI): $(P - H)^+$ *m*/*z* 665, 2 Mo, 1 Fe, and 5 B atoms, loss of one H; fragment peaks corresponding to sequential loss of three CO. *m*/*z*: calcd for the weighted average of those isotopomers with the formula $C_{23}H_{39}B_5FeMo_2O_3$ falling within the resolution limits of the spectrometer at the measured ion peak, 670.0822; obsd, 670.0820. IR (KBr, cm^{-1}): 2992 w, sh, 2959 m, 2921 w, 2862 vw, sh, ν(C−H); 2479 m, 2467 m, sh, 2423 w, ν(B−H$_t$); 1994 vs, 1947 s, 1934 s, ν(C−O); 1074 m, δ(CH$_3$); 719 w, 649 m, ρ(CH$_3$) [δ = deformation mode, ρ = rocking mode]. Further spectroscopic data are given in Tables 1−3.

X-ray Structure Determinations. Details of the data collection and structure refinement procedures for compounds **2**−**4** and **6** are summarized in Table 4. Data collection for compounds **3**, **4**, and **6** was carried out using an Enraf-Nonius CAD4 diffractometer; that for **2** was carried out on an Enraf-Nonius FAST area detector diffractometer. All data were collected at room temperature.

(Cp*Cr)$_2$B$_5$H$_9$ (2). A brown platelike crystal grown by slow cooling of a hexane solution of **2** to −40 °C was mounted on a glass fiber for data collection. The structure was solved by direct methods (SHELXS-86[26]), and all non-hydrogen atoms were found in an *E* map. After the non-hydrogen atoms were refined anisotropically to convergence, all hydrogen atoms were located in a difference Fourier map. Both borane and methyl hydrogens were included in the final refinement, the former being treated isotropically and the latter being treated as idealized riding atoms [r(C−H) = 0.96 Å, U_{iso}(H) = 1.5U_{eq}(C)]. The structure was refined on F^2 by full-matrix least-squares methods using SHELXTL V5.[27] Coordinates and selected bond distances are given in Tables S2 (Supporting Information) and 5, respectively.

(Cp*Cr)$_2$B$_4$H$_8$Fe(CO)$_3$ (3). A dark brown acicular crystal grown by slow diffusion of hexane into a toluene solution of **3** held at 5 °C was mounted on a glass fiber for data collection. The structure was solved by direct methods (SHELXS-86[26]), and the metal atoms and most other non-hydrogen atoms were found in an *E* map. The remaining non-hydrogen atoms were found in a successive difference Fourier synthesis. All non-hydrogen atoms were refined anisotropically, and all hydrogen atoms were then located in a difference Fourier map. Both borane and methyl hydrogens were included in the final refinement, the former being treated isotropically and the latter being treated as idealized riding atoms [r(C−H) = 0.96 Å, U_{iso}(H) = 1.5U_{eq}(C)]. The structure was refined on F^2 by full-matrix least-squares methods using SHELXL-93.[28] Coordinates and selected bond distances are given in Tables S2 (Supporting Information) and 6, respectively. Other data were deposited in conjunction with the original communication.[15]

(Cp*Cr)$_2$B$_4$H$_7$Co(CO)$_3$ (4). A dark brown platelike crystal suitable for X-ray diffraction was grown by cooling a hexane solution of **4** to −40 °C and mounted on a glass fiber prior to data collection. Most of the non-hydrogen atoms were located by direct methods, and the remainder of the atoms were found in a successive difference Fourier synthesis. All non-hydrogen atoms were refined anisotropically, and all hydrogen atoms were then located in a difference Fourier map. Both borane and methyl hydrogens were included in the final refinement, the former being treated isotropically with bond length restraints and the latter being treated as idealized riding atoms [r(C−H) = 0.96 Å, U_{iso}(H) = 1.5U_{eq}(C)]. The structure was refined on F^2 by full-matrix least-squares methods using SHELXTL V5.[27] Coordinates and selected bond distances are given in Tables S2 (Supporting Information) and 7, respectively.

(Cp*Mo)$_2$B$_5$H$_9$Fe(CO)$_3$ (6). An orange acicular crystal suitable for X-ray diffraction was grown by slow evaporation of solvent from a toluene solution of **6** over a period of 3−4 days and mounted on a glass fiber. Most of the non-hydrogen atoms were located by direct methods, and the remainder were found in a successive difference Fourier synthesis. All non-hydrogen atoms were refined anisotropically, and all hydrogen atoms were then located in a difference Fourier map. Both borane and methyl hydrogens were included in the final refinement, bridging hydrogens being treated isotropically with bond length restraints and terminal hydrogens being treated as idealized riding atoms. The structure was refined on F^2 by full-matrix least-squares methods using SHELXTL V5.[27] Coordinates and selected bond distances are given in Tables S2 (Supporting Information) and 8, respectively.

Table 5. Selected Interatomic Distances (Å) and Angles (deg) for (Cp*Cr)$_2$B$_5$H$_9$ (**2**)

Distances			
Cr(1)−B(1)	2.193(7)	B(4)−H(6)	1.07(5)
Cr(1)−B(2)	2.118(5)	B(5)−H(7)	1.27(4)
Cr(1)−B(3)	2.109(5)	B(5)−H(8)	1.24(5)
Cr(1)−B(4)	2.120(6)	B(5)−H(9)	1.14(5)
Cr(1)−B(5)	2.206(7)	Cr(2)−C(12)	2.192(4)
Cr(1)−C(1)	2.194(4)	Cr(2)−C(13)	2.189(4)
Cr(1)−C(2)	2.208(4)	Cr(2)−C(14)	2.210(4)
Cr(1)−C(3)	2.193(5)	Cr(2)−C(15)	2.217(4)
Cr(1)−C(4)	2.183(5)	Cr(2)−H(2)	1.77(7)
Cr(1)−C(5)	2.189(4)	Cr(2)−H(8)	1.74(5)
Cr(1)−H(1)	1.65(6)	B(1)−B(2)	1.694(10)
Cr(1)−H(7)	1.80(5)	B(1)−H(1)	1.29(6)
Cr(1)−Cr(2)	2.6246(9)	B(1)−H(2)	1.26(7)
Cr(2)−B(1)	2.199(7)	B(1)−H(3)	1.23(8)
Cr(2)−B(2)	2.106(5)	B(2)−B(3)	1.669(9)
Cr(2)−B(3)	2.107(5)	B(2)−H(4)	1.08(5)
Cr(2)−B(4)	2.108(6)	B(3)−B(4)	1.661(9)
Cr(2)−B(5)	2.201(6)	B(3)−H(5)	1.09(6)
Cr(2)−C(11)	2.205(4)	B(4)−B(5)	1.665(11)
Angles			
C(1)−Cr(1)−B(1)	154.8(2)	B(1)−Cr(1)−B(3)	86.7(2)
C(1)−Cr(1)−B(2)	149.7(2)	B(1)−Cr(1)−B(4)	104.8(2)
C(1)−Cr(1)−B(3)	117.7(2)	B(1)−Cr(1)−B(5)	89.0(3)
C(1)−Cr(1)−B(4)	97.2(2)	B(2)−Cr(1)−B(3)	46.5(2)
C(1)−Cr(1)−B(5)	98.3(2)	B(2)−Cr(1)−B(4)	85.7(2)
C(2)−Cr(1)−B(1)	152.0(3)	B(2)−Cr(1)−B(5)	104.7(2)
C(2)−Cr(1)−B(2)	113.8(2)	B(3)−Cr(1)−B(4)	46.2(3)
C(2)−Cr(1)−B(3)	87.5(2)	B(3)−Cr(1)−B(5)	85.7(3)
C(2)−Cr(1)−B(4)	90.6(2)	B(4)−Cr(1)−B(5)	45.2(3)
C(2)−Cr(1)−B(5)	117.9(3)	B(2)−B(1)−Cr(1)	64.6(3)
C(3)−Cr(1)−B(1)	115.7(3)	Cr(1)−B(1)−Cr(2)	73.4(2)
C(3)−Cr(1)−B(2)	90.7(2)	B(1)−B(2)−B(3)	123.0(5)
C(3)−Cr(1)−B(3)	91.0(2)	B(1)−B(2)−Cr(1)	69.2(3)
C(3)−Cr(1)−B(4)	118.5(3)	B(3)−B(2)−Cr(1)	66.5(3)
C(3)−Cr(1)−B(5)	154.9(3)	Cr(1)−B(2)−Cr(2)	76.8(2)
C(4)−Cr(1)−B(1)	100.0(2)	B(2)−B(3)−B(4)	119.9(4)
C(4)−Cr(1)−B(2)	104.5(2)	B(2)−B(3)−Cr(1)	67.0(3)
C(4)−Cr(1)−B(3)	126.3(2)	B(4)−B(3)−Cr(1)	67.2(3)
C(4)−Cr(1)−B(4)	153.0(2)	Cr(1)−B(3)−Cr(2)	77.0(2)
C(4)−Cr(1)−B(5)	146.8(3)	B(3)−B(4)−B(5)	124.0(5)
C(5)−Cr(1)−B(1)	118.7(2)	B(3)−B(4)−Cr(1)	66.5(3)
C(5)−Cr(1)−B(2)	141.3(2)	B(5)−B(4)−Cr(1)	70.1(4)
C(5)−Cr(1)−B(3)	148.7(2)	Cr(1)−B(4)−Cr(2)	76.7(2)
C(5)−Cr(1)−B(4)	130.7(2)	B(4)−B(5)−Cr(1)	64.7(3)
C(5)−Cr(1)−B(5)	110.8(2)	Cr(1)−B(5)−Cr(2)	73.1(2)
B(1)−Cr(1)−B(2)	46.2(3)		

MO Calculations. Fenske−Hall calculations[17,18] were carried out for the molecules $(CpM)_2B_4H_8$ [M = Cr (**1′**), or Mo (**7′**)] and $(CpM)_2B_5H_9$ [M = Cr (**2′**), Mo (**5′**)] and for the mixed-metal clusters $(CpCr)_2B_4H_8Fe(CO)_3$ (**3′**) and $(CpCr)_2B_4H_7Co(CO)_3$ (**4′**). In all cases except **7′**, the geometry used was that derived from the solid-state structure determination of the corresponding Cp* (η^5-C$_5$Me$_5$) [for **1′**, **2′**, **3′**, and **4′**] or Cp′ (η^5-C$_5$H$_4$Me) derivative [for **5′**] (including hydrogen atom positions) with the simplification that the methylated Cp* or Cp′ ligand was replaced by Cp (η^5-C$_5$H$_5$).[15,24] In the case of **7′**, a molecule not yet isolated, the geometry used was that for the analogous chromium compound (**1′**) with molybdenum atoms transposed for chromium. For the molecules $(CpM)_2B_4H_8$ [M = Cr (**1′**), Mo (**7′**)] and $(CpM)_2B_5H_9$ [M = Cr (**2′**), Mo (**5′**)], the minimal atomic orbital (AO) basis set calculations were transformed into fragment basis sets for 2 CpM and

(26) Sheldrick, G. M. *Acta Crystallogr.* **1990**, *A46*, 467.
(27) *SHELXTL-V5*; Siemens Industrial Automation Inc.: Madison, WI, 1994.
(28) Sheldrick, G. M. *SHELXL93*; University of Göttingen: Göttingen, Germany, 1993.

Table 6. Selected Interatomic Distances (Å) and Angles (deg) for $(Cp^*Cr)_2B_4H_8Fe(CO)_3$ (**3**)

Distances			
Fe−C(23)	1.765(9)	Cr(2)−B(4)	2.190(8)
Fe−C(22)	1.779(8)	Cr(2)−C(11)	2.239(6)
Fe−C(21)	1.787(8)	Cr(2)−C(12)	2.209(6)
Fe−Cr(2)	2.7398(13)	Cr(2)−C(13)	2.232(6)
Fe−Cr(1)	2.7457(13)	Cr(2)−C(14)	2.235(6)
Fe−B(1)	2.181(8)	Cr(2)−C(15)	2.222(6)
Fe−H(2)	1.58(7)	Cr(2)−H(3)	1.77(6)
Fe−H(3)	1.65(7)	Cr(2)−H(8)	1.67(6)
Cr(1)−B(1)	2.250(8)	C(21)−O(1)	1.140(8)
Cr(1)−B(2)	2.090(7)	C(22)−O(2)	1.152(8)
Cr(1)−B(3)	2.093(7)	C(23)−O(3)	1.149(9)
Cr(1)−B(4)	2.178(8)	B(1)−B(2)	1.715(10)
Cr(1)−C(1)	2.217(6)	B(1)−H(1)	1.11(5)
Cr(1)−C(2)	2.244(6)	B(1)−H(2)	1.34(7)
Cr(1)−C(3)	2.230(6)	B(1)−H(3)	1.24(7)
Cr(1)−C(4)	2.226(6)	B(2)−B(3)	1.696(10)
Cr(1)−C(5)	2.235(6)	B(2)−H(4)	1.05(5)
Cr(1)−H(2)	1.89(6)	B(3)−B(4)	1.753(10)
Cr(1)−H(7)	1.69(6)	B(3)−H(5)	1.12(5)
Cr(1)−Cr(2)	2.7099(13)	B(4)−H(6)	1.09(6)
Cr(2)−B(1)	2.263(8)	B(4)−H(7)	1.15(7)
Cr(2)−B(2)	2.104(7)	B(4)−H(8)	1.19(6)
Cr(2)−B(3)	2.094(7)		

Angles			
C(23)−Fe−C(22)	97.1(4)	B(1)−Cr(1)−B(4)	104.8(3)
C(23)−Fe−C(21)	94.6(3)	B(2)−Cr(1)−B(3)	47.8(3)
C(22)−Fe−C(21)	99.7(3)	B(2)−Cr(1)−B(4)	88.5(3)
Cr(2)−Fe−Cr(1)	59.21(3)	B(3)−Cr(1)−B(4)	48.4(3)
B(1)−Cr(1)−C(1)	94.7(3)	B(1)−Cr(1)−Fe	50.6(2)
B(2)−Cr(1)−C(1)	90.7(3)	B(2)−Cr(1)−Fe	91.4(2)
B(3)−Cr(1)−C(1)	113.9(3)	B(3)−Cr(1)−Fe	109.8(2)
B(4)−Cr(1)−C(1)	151.8(3)	B(4)−Cr(1)−Fe	86.5(2)
B(1)−Cr(1)−C(2)	106.3(2)	Cr(2)−Cr(1)−Fe	60.29(3)
B(2)−Cr(1)−C(2)	124.4(3)	O(1)−C(21)−Fe	169.1(6)
B(3)−Cr(1)−C(2)	147.2(3)	O(2)−C(22)−Fe	177.7(7)
B(4)−Cr(1)−C(2)	145.3(3)	O(3)−C(23)−Fe	173.1(7)
B(1)−Cr(1)−C(3)	141.7(3)	B(2)−B(1)−Fe	126.8(5)
B(2)−Cr(1)−C(3)	149.2(3)	B(2)−B(1)−Cr(1)	61.9(3)
B(3)−Cr(1)−C(3)	128.6(3)	Cr(1)−B(1)−Cr(2)	73.8(2)
B(4)−Cr(1)−C(3)	109.1(3)	B(1)−B(2)−B(3)	123.7(6)
B(1)−Cr(1)−C(4)	154.4(3)	B(1)−B(2)−Cr(1)	71.7(4)
B(2)−Cr(1)−C(4)	118.9(3)	B(3)−B(2)−Cr(1)	66.2(3)
B(3)−Cr(1)−C(4)	92.6(3)	Cr(1)−B(2)−Cr(2)	80.5(3)
B(4)−Cr(1)−C(4)	94.3(3)	B(2)−B(3)−B(4)	119.4(6)
B(1)−Cr(1)−C(5)	117.6(3)	B(2)−B(3)−Cr(1)	66.0(3)
B(2)−Cr(1)−C(5)	87.9(3)	B(4)−B(3)−Cr(1)	68.3(4)
B(3)−Cr(1)−C(5)	85.6(3)	Cr(1)−B(3)−Cr(2)	80.6(3)
B(4)−Cr(1)−C(5)	115.2(3)	B(3)−B(4)−Cr(1)	63.3(3)
B(1)−Cr(1)−B(2)	46.4(3)	Cr(1)−B(4)−Cr(2)	76.7(3)
B(1)−Cr(1)−B(3)	87.6(3)		

Table 7. Selected Interatomic Distances (Å) and Angles (deg) for $(Cp^*Cr)_2B_4H_7Co(CO)_3$ (**4**)

Distances			
Co−Cr(1)	2.673(2)	Cr(2)−B(4)	2.205(10)
Co−Cr(2)	2.652(2)	Cr(2)−C(11)	2.240(7)
Co−C(21)	1.738(9)	Cr(2)−C(12)	2.226(7)
Co−C(23)	1.743(12)	Cr(2)−C(13)	2.238(7)
Co−C(22)	1.770(12)	Cr(2)−C(14)	2.226(7)
Co−B(1)	2.090(10)	Cr(2)−C(15)	2.230(8)
Co−H(12)	1.55(7)	Cr(2)−C(21)	2.497(8)
Cr(1)−B(1)	2.209(9)	Cr(2)−H(43)	1.70(5)
Cr(1)−B(2)	2.062(9)	C(21)−O(21)	1.168(10)
Cr(1)−B(3)	2.064(9)	C(22)−O(22)	1.132(13)
Cr(1)−B(4)	2.196(10)	C(23)−O(23)	1.153(12)
Cr(1)−C(1)	2.209(7)	B(1)−B(2)	1.684(13)
Cr(1)−C(2)	2.202(7)	B(1)−H(11)	1.08(5)
Cr(1)−C(3)	2.226(7)	B(1)−H(12)	1.22(5)
Cr(1)−C(4)	2.204(7)	B(2)−B(3)	1.683(13)
Cr(1)−C(5)	2.222(7)	B(2)−H(21)	1.09(5)
Cr(1)−H(12)	1.73(5)	B(3)−B(4)	1.718(14)
Cr(1)−H(42)	1.70(5)	B(3)−H(31)	1.05(5)
Cr(1)−Cr(2)	2.694(2)	B(4)−H(41)	1.07(5)
Cr(2)−B(1)	2.196(9)	B(4)−H(42)	1.19(4)
Cr(2)−B(2)	2.114(9)	B(4)−H(43)	1.19(5)
Cr(2)−B(3)	2.089(10)		

Angles			
B(1)−Cr(1)−C(1)	144.8(4)	B(3)−Cr(1)−B(4)	47.4(4)
B(2)−Cr(1)−C(1)	150.2(3)	C(21)−Cr(2)−Co	39.3(2)
B(3)−Cr(1)−C(1)	127.1(4)	C(21)−Co−Cr(2)	65.5(3)
B(4)−Cr(1)−C(1)	106.3(4)	O(21)−C(21)−Co	157.8(8)
B(1)−Cr(1)−C(2)	154.2(3)	Co−C(21)−Cr(2)	75.1(3)
B(2)−Cr(1)−C(2)	118.0(3)	O(21)−C(21)−Cr(2)	127.1(7)
B(3)−Cr(1)−C(2)	92.9(4)	O(22)−C(22)−Co	177.6(11)
B(4)−Cr(1)−C(2)	94.3(3)	O(23)−C(23)−Co	177.7(12)
B(1)−Cr(1)−C(3)	117.7(3)	C(21)−Co−C(23)	101.9(5)
B(2)−Cr(1)−C(3)	88.3(3)	C(21)−Co−C(22)	97.1(5)
B(3)−Cr(1)−C(3)	88.0(3)	C(23)−Co−C(22)	104.2(6)
B(4)−Cr(1)−C(3)	116.4(4)	Cr(2)−Co−Cr(1)	60.79(4)
B(1)−Cr(1)−C(4)	96.0(3)	B(2)−B(1)−Co	128.4(6)
B(2)−Cr(1)−C(4)	93.2(3)	B(2)−B(1)−Cr(1)	62.2(4)
B(3)−Cr(1)−C(4)	118.0(3)	Cr(2)−B(1)−Cr(1)	75.4(3)
B(4)−Cr(1)−C(4)	153.3(3)	B(1)−B(2)−B(3)	121.7(7)
B(1)−Cr(1)−C(5)	109.1(3)	B(1)−B(2)−Cr(1)	71.5(4)
B(2)−Cr(1)−C(5)	127.6(4)	B(3)−B(2)−Cr(1)	66.0(4)
B(3)−Cr(1)−C(5)	149.5(3)	Cr(1)−B(2)−Cr(2)	80.4(3)
B(4)−Cr(1)−C(5)	142.3(4)	B(2)−B(3)−B(4)	121.9(7)
B(1)−Cr(1)−B(2)	46.3(3)	B(2)−B(3)−Cr(1)	65.9(4)
B(1)−Cr(1)−B(3)	86.9(4)	B(4)−B(3)−Cr(1)	70.3(5)
B(1)−Cr(1)−B(4)	104.2(3)	Cr(1)−B(3)−Cr(2)	80.9(3)
B(2)−Cr(1)−B(3)	48.1(4)	B(3)−B(4)−Cr(1)	62.3(4)
B(2)−Cr(1)−B(4)	88.5(4)	Cr(1)−B(4)−Cr(2)	75.5(3)

B_nH_{n+4} fragments (n = 4, 5). For the mixed-metal species **3′** and **4′**, transformation was carried out into a fragment basis for $M(CO)_3$ and $(CpCr)_2B_4H_n$ fragments (n = 8, M = Fe; n = 7, M = Co).

Results

Synthesis and Characterization. The results of the reactions of group 6 metallaboranes with the monoboron species BH_3·thf and $BHCl_2$·SMe_2 and with the metal carbonyls $Fe_2(CO)_9$ and $Co_2(CO)_8$ are summarized in Scheme 1. The structures shown are based on the analyses of the spectroscopic and crystallographic data which follow.

$(Cp^*Cr)_2B_5H_9$ (2). The reaction of **1** with $BHCl_2$·SMe_2 leads to the isolation of a single metallaborane; the mass spectral data are consistent with the composition $(Cp^*Cr)_2B_5H_9$, and the NMR data suggest a diamagnetic compound. The ^{11}B NMR data indicate the presence of a pair of equivalent borons and a unique boron, each linked directly to a metal center, and a single terminal hydrogen and another pair of equivalent borons, each linked to two bridging hydrogens and one terminal hydrogen. Furthermore, the ^1H and ^{13}C NMR spectra imply two equivalent Cp* ligands, four equivalent CrHB protons, and three distinct BH_t groups (2:2:1). These NMR data are consistent with the molecular geometry shown in Scheme 1, a finding reinforced by similar spectra reported for the structurally characterized species $(C_5H_4MeMo)_2B_5H_9$.[24] Attempts to probe the mechanism of addition of the BH fragment to **1** (e.g., direct insertion into a B−B bond or coordination to the open face of the cluster followed by migration of bridging hydrogens) by the use of "labeled" monoboron reagents such as $PhBCl_2$, BCl_3·SMe_2, or $[(thex)BH_2]_2$ [thex = $Me_2C(H)CMe_2$] met either with cluster degradation in the case of $PhBCl_2$ or BCl_3·SMe_2[29] or with little net reaction.

The single-crystal X-ray diffraction structure of **2** is shown in Figure 1 and confirms the structural inferences made on the basis of spectroscopic results. Selected interatomic distances

(29) Aldridge, S.; Shang, M.; Fehlner, T. P. *Acta Crystallogr.* **1998**, *C54*, 47.

Table 8. Selected Interatomic Distances (Å) and Angles (deg) for $(Cp^*Mo)_2B_5H_9Fe(CO)_3$ (**6**)

Distances			
Fe−C(1)	1.756(8)	Mo(2)−C(21)	2.334(6)
Fe−C(3)	1.770(8)	Mo(2)−C(22)	2.425(7)
Fe−C(2)	1.774(10)	Mo(2)−C(23)	2.385(6)
Fe−B(3)	2.156(8)	Mo(2)−C(24)	2.313(7)
Fe−B(2)	2.158(9)	Mo(2)−C(25)	2.284(7)
Fe−B(1)	2.175(8)	Mo(2)−H(3)	1.68(4)
Fe−Mo(1)	2.7454(12)	Mo(2)−H(9)	1.70(4)
Fe−Mo(2)	2.7525(12)	C(1)−O(1)	1.175(10)
Mo(1)−B(1)	2.364(8)	C(2)−O(2)	1.159(11)
Mo(1)−B(3)	2.157(8)	C(3)−O(3)	1.144(10)
Mo(1)−B(4)	2.309(8)	B(1)−H(1)	0.99(8)
Mo(1)−B(5)	2.271(8)	B(1)−H(2)	1.15(4)
Mo(1)−C(11)	2.368(7)	B(1)−H(3)	1.15(4)
Mo(1)−C(12)	2.379(8)	B(2)−B(3)	1.759(12)
Mo(1)−C(13)	2.330(8)	B(2)−B(4)	1.744(13)
Mo(1)−C(14)	2.299(7)	B(2)−H(4)	1.02(9)
Mo(1)−C(15)	2.334(7)	B(3)−B(4)	1.734(12)
Mo(1)−H(2)	1.69(4)	B(3)−H(5)	1.25(8)
Mo(1)−H(8)	1.72(4)	B(4)−B(5)	1.795(13)
Mo(1)−Mo(2)	2.9408(9)	B(4)−H(6)	0.77(9)
Mo(2)−B(1)	2.355(8)	B(5)−H(7)	1.23(8)
Mo(2)−B(2)	2.154(9)	B(5)−H(8)	1.16(4)
Mo(2)−B(4)	2.299(9)	B(5)−H(9)	1.15(4)
Mo(2)−B(5)	2.259(8)		

Angles			
C(1)−Fe−C(3)	96.0(4)	B(4)−Mo(1)−C(15)	104.6(3)
C(1)−Fe−C(2)	96.4(4)	B(5)−Mo(1)−C(15)	90.4(3)
C(3)−Fe−C(2)	94.4(4)	B(1)−Mo(1)−B(3)	98.0(3)
B(1)−Fe−B(2)	103.9(3)	B(1)−Mo(1)−B(4)	99.3(3)
B(2)−Fe−B(3)	48.1(3)	B(1)−Mo(1)−B(5)	92.1(3)
B(1)−Fe−B(3)	104.1(3)	B(3)−Mo(1)−B(4)	45.6(3)
Mo(1)−Fe−Mo(2)	64.67(3)	B(3)−Mo(1)−B(5)	91.6(3)
B(1)−Mo(1)−C(11)	159.0(3)	B(4)−Mo(1)−B(5)	46.1(3)
B(3)−Mo(1)−C(11)	82.0(3)	Mo(2)−B(1)−Mo(1)	77.1(3)
B(4)−Mo(1)−C(11)	95.6(3)	B(3)−B(2)−B(4)	59.4(5)
B(5)−Mo(1)−C(11)	108.9(3)	B(2)−B(3)−B(4)	59.9(5)
B(1)−Mo(1)−C(12)	125.2(3)	B(2)−B(3)−Mo(1)	106.1(5)
B(3)−Mo(1)−C(12)	84.7(3)	B(4)−B(3)−Mo(1)	71.9(4)
B(4)−Mo(1)−C(12)	118.6(3)	B(2)−B(4)−B(4)	60.8(5)
B(5)−Mo(1)−C(12)	142.6(3)	B(3)−B(4)−B(5)	128.3(6)
B(1)−Mo(1)−C(13)	105.3(3)	B(2)−B(4)−B(5)	128.1(6)
B(3)−Mo(1)−C(13)	116.4(3)	B(2)−B(4)−Mo(1)	100.7(5)
B(4)−Mo(1)−C(13)	151.9(3)	B(3)−B(4)−Mo(1)	62.6(4)
B(5)−Mo(1)−C(13)	143.7(3)	B(5)−B(4)−Mo(1)	65.8(4)
B(1)−Mo(1)−C(14)	115.3(3)	Mo(2)−B(4)−Mo(1)	79.3(3)
B(3)−Mo(1)−C(14)	139.5(3)	B(4)−B(5)−Mo(1)	68.0(3)
B(4)−Mo(1)−C(14)	139.0(3)	Mo(2)−B(5)−Mo(1)	80.9(2)
B(5)−Mo(1)−C(14)	108.5(3)	O(1)−C(1)−Fe	177.3(8)
B(1)−Mo(1)−C(15)	148.9(3)	O(2)−C(2)−Fe	174.7(8)
B(3)−Mo(1)−C(15)	112.9(3)	O(3)−C(3)−Fe	175.9(8)

and angles are listed in Table 5. Superficially this structure resembles a hexagonal bipyramid with a single missing equatorial vertex but, given the electron count of six sep's, is probably more accurately thought of as a bicapped trigonal bipyramid. A similar structural interpretation has been suggested for $(C_5H_4MeMo)_2B_5H_9$,[24] and in each case the trigonal bipyramidal $M_2B_3H_3$ unit is capped by two BH_3 units over the M_2B faces. Such an interpretation implies a single bond between the chromium centers, and the Cr−Cr distance (2.63 Å) is consistent with this.[30] The similarity in the structures of **2** and $(C_5H_4MeMo)_2B_5H_9$ is striking—differences in M−M and various M−B distances can be accounted for simply by the larger size (≈0.1 Å larger) of the Mo(II) center compared to that of Cr(II).[31] Average B−B distances are also similar. The geometries of **2** and $(C_5H_4MeMo)_2B_5H_9$ *do* differ slightly with respect to

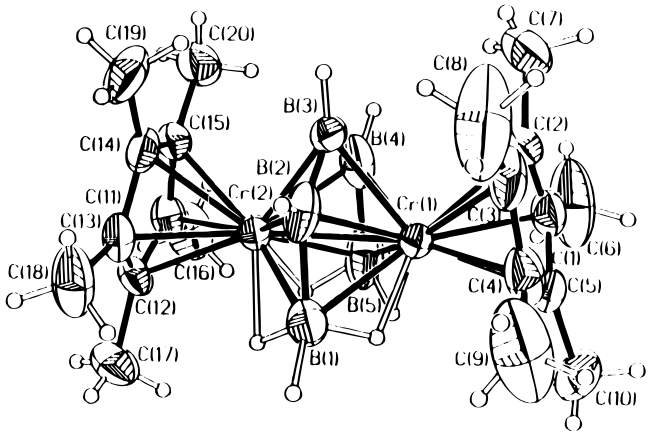

Figure 1. ORTEP drawing of $(Cp^*Cr)_2B_5H_9$ (**2**).

Scheme 1

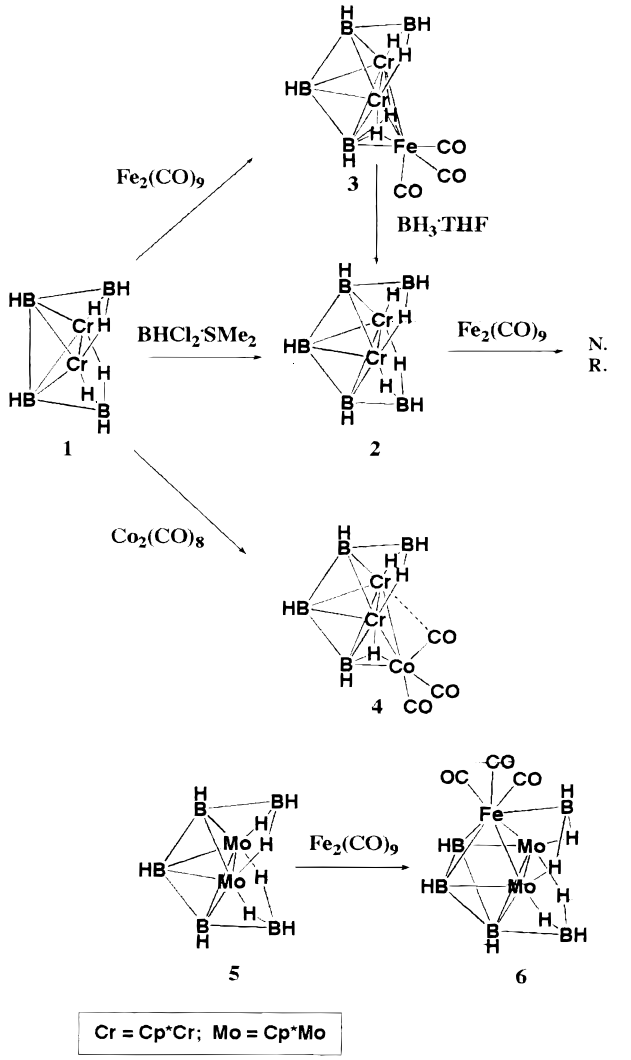

the size of the open face of the cluster [defined by the cyclic M(μ-H)B(μ-H)M(μ-H)B(μ-H) fragment]; this face is somewhat more open in the case of the molybdenum compound [*r*(M−M) = 2.81 vs 2.63 Å for **2**; *r*(B···B) = 3.27 vs 3.08 Å for **2**],[24] a factor which may contribute to the differing reactivities of Cr_2B_5 and Mo_2B_5 clusters discussed below.

(30) See, for example: Adams, R. D.; Collins, D. E.; Cotton, F. A. *J. Am. Chem. Soc.* **1974**, *96*, 749.

(31) Huheey, J. E. *Inorganic Chemistry. Principles of Structure and Reactivity*; Harper and Row: New York, 1972.

Comparison of the structure of **2** with that of **1**, from which it is formally derived by insertion of a B−H unit into a B−B bond, reveals several contrasting features. Not only is the Cr−Cr distance significantly shorter in **2** than in **1** (2.63 vs 2.88 Å [12]) but the Cr−B linkages (both hydrogen-bridged and directly bonded) are noticeably longer and the B−B−B angles somewhat wider. In effect, the cluster framework has been deformed by compression along the Cr−Cr axis and elongation perpendicular to it. These geometric changes mirror the "squashing" of the cluster framework on going from the unsaturated species **1** to the saturated derivatives $(Cp^*Cr)_2B_4H_8Fe(CO)_3$ and $(Cp^*Cr)_2B_4H_6(CO)_2$.[16] The electronic factors underlying these structural differences are discussed below.

An alternative interpretation of the structure of **2** is as a triple-decker sandwich compound, the three layers comprising the two Cp* rings and the B_5 unit. In general, the Cr−Cr distance is somewhat shorter than those typically reported for first-row triple-decker compounds [e.g.: $(CpCo)_2C_2B_3H_5$, 3.14 Å;[32] $(CpFe)_2R_2C(BMe)_2S$, 3.24 Å[33] (Cp = η^5-C_5H_5)] although very similar to that found in the recently synthesized chromium species $(CpCr)_2B_4H_4C_2(C_3H_6)$ (2.66 Å), which contains a planar C_2B_4-based ligand as the middle "deck".[34] There is, however, significant tilting of the Cp* planes in **2** away from the open face of the B_5 ligand [the angle between them being 29.7(2)°]; such a feature is not observed for typical triple-decker compounds but is common to chromaboranes derived from the unsaturated species **1**.[12] As such, interpretation of **2** as a trigonal bipyramidal metallaborane cluster rather than as a triple-decker organometallic complex is probably more realistic.

$(Cp^*Cr)_2B_4H_8Fe(CO)_3$ (3). The reaction of **1** with $Fe_2(CO)_9$ produces a single metallaborane product in 76% yield, with $Fe(CO)_5$ being the only identifiable iron carbonyl coproduct.[35] The mass spectrum implies the composition $(Cp^*Cr)_2B_4H_8Fe(CO)_3$, suggesting addition of an $Fe(CO)_3$ fragment to **1**.[15] NMR spectra imply a diamagnetic compound. At low temperature, the existence of four distinct ^{11}B signals as well as a single Cp* signal, two broad overlapping terminal BH resonances, and two Cr−H−B signals in the ^{1}H spectrum implies asymmetric coordination of the $Fe(CO)_3$ unit to a $(Cp^*Cr)_2B_4H_8$ framework, such that only one of the two planes of symmetry present in **1** is retained. Terminal BH and CO stretching frequencies are observed in the solid-state IR spectrum, and the presence of the latter is confirmed by the ^{13}C NMR spectrum.

The single-crystal X-ray diffraction structure of **3** is shown in Figure 2; relevant interatomic distances and angles are listed in Table 6. The structure is consistent with the low-temperature NMR data and can be viewed as a six-sep trigonal bipyramidal cluster in which the central Cr_2B_3 unit is capped on one Cr_2B face by a BH_3 fragment and on the other by $Fe(CO)_3$. In this way, the structure of **3** is analogous to that of **2** with the capping position occupied by one of the BH units instead filled by the isolobal $Fe(CO)_3$ fragment; the Cr−Cr distances for each cluster are similar (2.63 Å for **2**; 2.71 Å for **3**) and markedly shorter than that found in **1** (2.88 Å).[12,15] Indeed, both **2** and **3** show similar lengthenings of Cr−B and B−B linkages compared to those of the unsaturated species **1**. Where **2** and **3** do differ is in the positioning of bridging hydrogen atoms; **2** contains two pairs of Cr−H−B linkages, and although one pair of Cr−H−B bonds is retained in **3**, the other hydrogens are μ_3 (Cr−Fe−B) face-bridging. Attachment of the $Fe(CO)_3$ fragment to the chromaborane cluster is via these two face-bridging hydrogens and a pair of Fe−Cr two-center two-electron bonds. This leads to an alternative view of **3** as a four-electron $(Cp^*Cr)_2B_4H_8$ ligand coordinated to an $Fe(CO)_3$ fragment.[16]

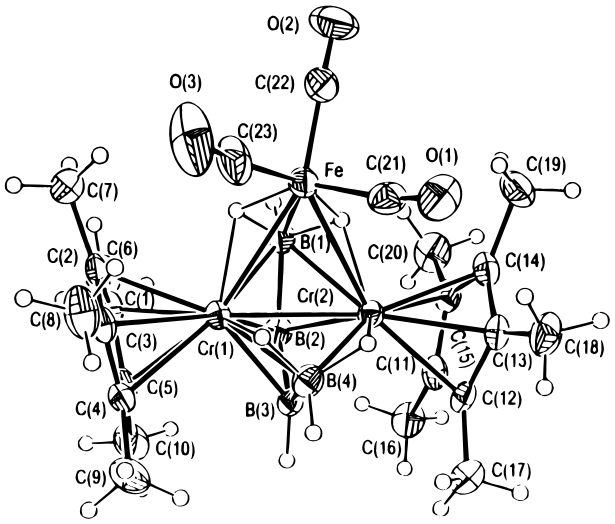

Figure 2. ORTEP drawing of $(Cp^*Cr)_2B_4H_8Fe(CO)_3$ (**3**).

If one views **3** as a complex between an organometallic fragment and a cluster ligand, the iron center attains an 18-electron configuration by forming two Fe−Cr bonds and by utilizing two BH→Fe donor−acceptor bonds in which the BH_2 group functions similarly to a bidentate borohydride[36] or an electron-rich neutral borane.[37−39] This type of interaction with the Cr−H−B hydrogens, taken to its extreme form, leads to hydride transfer, as seen in the reduction of CS_2 to the CH_2S_2 ligand by **1**.[40] The fluxionality of **3** at higher temperatures is then derived from interaction of the iron center with each of the two BH_2 groups of the $(Cp^*Cr)_2B_4H_8$ moiety—these being equivalent in the free ligand. In essence, the $Fe(CO)_3$ unit "swings" back and forth between the two BH_2 units such that at 80 °C the two boron signals at δ_B 129.5 and 105.8 coalesce into a single resonance at δ_B 117.5 and those at δ_B 46.0 and 4.1 coalesce into one at δ_B 27.3. In addition, the two Cr−H−B signals (δ_H −16.2 and −8.0 at −20 °C) disappear into the baseline at 22 °C before coalescing into a single peak at δ_H −11.9 at 50 °C. The free energy of activation calculated for this process on the basis of either ^{1}H or ^{11}B NMR spectra is on the order of 51 kJ mol^{-1}.

Examination of the stretching frequencies for the carbonyl ligands provides corroboration for the view of **3** as a coordination complex featuring a cluster as a ligand. These are in the frequency range typically associated with ferraborane anions, being some 100 cm^{-1} lower than those of any neutral ferraborane.[41−43] This is consistent with a buildup of negative

(32) Beer, D. C.; Miller, V. R.; Sneddon, L. G.; Grimes, R. N.; Mathew, M.; Palenik, G. L *J. Am. Chem. Soc.* **1973**, *95*, 3046.
(33) Seibert, W.; Renk, T.; Kinberger, K.; Bochmann, M.; Krüger, C. *Angew. Chem., Int. Ed. Engl.* **1976**, *15*, 779.
(34) Kawamura, K.; Shang, M.; Fehlner, T. P. *Inorg. Chem.*, in press.
(35) Nakamoto, K. *Infrared and Raman Spectra of Inorganic and Coordination Compounds*; Wiley-Interscience: New York, 1990.
(36) Marks, T. J.; Kolb, J. R. *Chem. Rev.* **1977**, *77*, 263.
(37) Katoh, K.; Shimoi, M.; Ogino, H. *Inorg. Chem.* **1992**, *31*, 670.
(38) Shimoi, M.; Katoh, K.; Ogino, H. *Chem. Commun.* **1990**, 811.
(39) Snow, S. A.; Shimoi, M.; Ostler, C. D.; Thompson, B. K.; Kodama, G.; Parry, R. W. *Inorg. Chem.* **1984**, *23*, 511.
(40) Hashimoto, H.; Shang, M.; Fehlner, T. P. *Organometallics* **1996**, *15*, 1963.
(41) Fehlner, T. P.; Housecroft, C. E.; Scheidt, W. R.; Wong, K. S. *Organometallics* **1983**, *2*, 825.
(42) Jacobsen, G. B.; Andersen, E. L.; Housecroft, C. L.; Hong, F.-E.; Buhl, M. L.; Long, G. J.; Fehlner, T. P. *Inorg. Chem.* **1987**, *26*, 4040.
(43) Vites, J. C.; Housecroft, C. E.; Eigenbrot, C.; Buhl, M. L.; Long, G. J.; Fehlner, T. P. *J. Am. Chem. Soc.* **1986**, *108*, 3304.

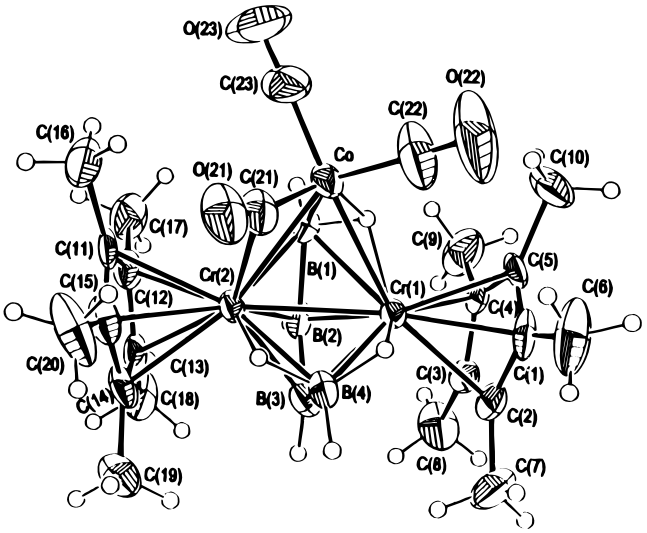

Figure 3. ORTEP drawing of $(Cp^*Cr)_2B_4H_7Co(CO)_3$ (**4**).

charge at the iron center also implied by the low-field ^{13}C chemical shift for the CO ligands and by the charge distribution calculated by Fenske−Hall methods.[16−18] Clearly, formation of σ donor−acceptor bonds with the hydridic Cr−H−B units causes significant charge transfer to the iron center.

$(Cp^*Cr)_2B_4H_7Co(CO)_3$ (4). Reaction of **1** with the dinuclear cobalt carbonyl, $Co_2(CO)_8$, leads to the isolation of a single metallaborane product for which the mass spectral data are consistent with the formulation $(Cp^*Cr)_2B_4H_7Co(CO)_3$. This suggests addition of a $Co(CO)_3$ fragment to **1** accompanied by loss of one hydrogen to give a cluster isoelectronic with **3**. ^{11}B NMR spectra show four signals at all temperatures, implying a static structure analogous to that seen for **3** at low temperature in solution and in the solid state. Furthermore, the existence of two high-field ^1H signals at δ −13.8 and −5.6 with the intensity ratio 1:2 implies that **4** features two Cr−H−B edge-bridging hydrogens and one Cr−Co−B−H face-bridging hydrogen. The principal carbonyl coproduct of the reaction was shown by IR to be $Co_4(CO)_{12}$.[44]

The single-crystal X-ray diffraction structure of **4** is shown in Figure 3; relevant interatomic distances and angles are listed in Table 7. The structure is consistent with the observed spectroscopic data and in gross geometric terms is analogous to that of **3**, with one of the two Cr−M−B face-bridging protons removed. **3** and **4** are isoelectronic, and **4** can therefore also be viewed as a six-sep bicapped trigonal bipyramidal cluster in which the two capping positions are occupied by BH and $Co(CO)_3$ fragments. In common with the other saturated chromaboranes **2** and **3**, **4** also shows significant shortening of the Cr−Cr bond and lengthening of Cr−B bonds when compared to the unsaturated species **1**. The electronic factors underlying these consistent geometric changes have been examined by Fenske−Hall methods with the results of the calculations discussed below.

4 can also be viewed as a complex between a transition metal fragment $[Co(CO)_3]$ and a three-electron cluster ligand $[(Cp^*Cr)_2B_4H_7]$. Formation of two Cr−Co bonds and a single donor−acceptor BH→Co linkage allows the cobalt center to attain an 18-electron configuration. In contrast to **3**, however, **4** is not fluxional at any temperature studied. The $(Cp^*Cr)_2B_4H_7$ ligand, having lost a bridging hydrogen atom, no longer has the pair of equivalent BH_2 groups present in **3**. In addition, **4** contains a semibridging carbonyl linkage between Co and Cr(2), the breakage of which would constitute an additional energy barrier to any fluxional process. The Co−C(21) and Cr(2)−C(21) distances (1.738 and 2.497 Å, respectively) and Co−C(21)−O(21) angle (157.8°) are consistent with a bent semibridging Co(μ-CO)Cr unit,[45] differing substantially from those reported for the symmetric bridging Co(μ-CO)Cr unit in $(OC)_3(Me_3P)Cr(\mu\text{-}t\text{-}Bu_2P)(\mu\text{-CO})Co(PMe_3)(CO)$ [r(Co−C) = 1.946 Å, r(Cr−C) = 1.984 Å, ∠(Co−C−O) = 131.0°].[46] The existence of a low-frequency CO stretching band at 1906 cm^{-1} in the IR spectrum of **4** is also consistent with the presence of a semibridging CO ligand.

$(Cp^*Mo)_2B_5H_9Fe(CO)_3$ (6). Reaction of **5** with a 6-fold excess of $Fe_2(CO)_9$ generates a single metallaborane product in yields of 48% based on the amount of **5** taken. In contrast to that of the reaction of $Fe_2(CO)_9$ with **1**, the iron carbonyl coproduct is $Fe_3(CO)_{12}$ (as identified by its IR spectrum[25]) rather than $Fe(CO)_5$. Mass spectral analysis is consistent with a compound of the formulation $(Cp^*Mo)_2B_5H_9Fe(CO)_3$, formed by addition of a single $Fe(CO)_3$ fragment to **5**. The ^1H and ^{11}B NMR data are, however, inconsistent with a complex analogous to **3** or **4** featuring an $M(CO)_3$ unit bound to the open face of the parent metallaborane—a static structure analogous to that of **3** in the solid state would imply five ^{11}B signals of equal intensity, whereas a rapidly fluxional species akin to that seen for **3** at higher temperatures in solution would give rise to three resonances (2:2:1). Four signals are observed in the ^{11}B NMR spectrum at δ_B +90.4, +41.4, +29.7, and −0.4 (2:1:1:1), together with a single Cp* resonance, two bridging hydrogen signals (δ_H −15.5 and −13.1; intensity 2:2), and three terminal BH signals (δ_H 8.0, 3.9, 0.9; 2:2:1) in the ^1H spectrum. These spectra are consistent with a structure based on a bicapped octahedral cluster—as would be expected for addition of a two-electron fragment to a six-sep bicapped trigonal bipyramid. Several possibilities exist as to the arrangement of metal and boron fragments about the vertexes of the cluster; of these, an Mo_2B_3Fe octahedron capped by two BH groups (as illustrated in Scheme 1) or a similar molecule in which the positions of the $Fe(CO)_3$ unit and one of the capping BH groups have been interchanged seems to be most plausible on the basis of the synthetic route employed.

Given this ambiguity in the interpretation of the spectroscopic results, a single-crystal X-ray diffraction study was carried out. The structure obtained is shown in Figure 4; relevant interatomic distances and angles are listed in Table 8. The structure is best viewed as a bicapped octahedron with Mo(1), Mo(2), B(2), and B(3) occupying the basal vertexes and Fe and B(4) the apical vertexes of the octahedron. This structure is then capped by a BH_3 unit on each of the two Mo_2B triangular faces. The change from the bicapped trigonal bipyramidal geometry observed for the six-sep species **5** to the bicapped octahedron observed for **6** is entirely in keeping with the changes predicted by the Wade/Mingos rules for the addition of a two-electron three-orbital fragment such as $Fe(CO)_3$.[47] The marked structural changes occurring on addition of a two-electron fragment to the saturated species **5** contrast sharply with the minor perturbation imposed upon the geometry of **1** on addition of the same two-electron fragment (to give **3**). This in turn provides support for the existence of delocalized unsaturation in **1**, as discussed below.

(44) Bor, G.; Sbrignadello, G.; Noack, K. *Helv. Chim. Acta* **1975**, *58*, 815.
(45) Crabtree, R. H.; Lavin, M. *Inorg. Chem.* **1986**, *25*, 805.
(46) Chandler, D. J.; Jones, R. A.; Stuart, A. L.; Wright, T. C. *Organometallics* **1984**, *3*, 1830.
(47) Wade, K. *New Scientist* **1974**, *62*, 615. Mingos, D. M. P. *Acc. Chem. Res.* **1984**, *17*, 311.

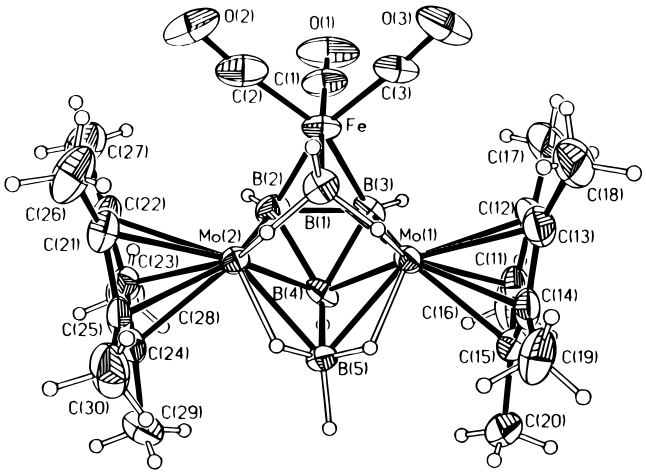

Figure 4. ORTEP drawing of $(Cp^*Mo)_2B_5H_9Fe(CO)_3$ (**6**).

The Mo−Mo bond length is somewhat longer than that found in $(C_5H_4MeMo)_2B_5H_9$ (2.94 Å as opposed to 2.81 Å)[24] although this is to be expected since the distribution of seven sep's among the various linkages of a bicapped octahedron leads to a lower formal bond order than is the case for the six sep's of a bicapped trigonal bipyramid. The Mo−Fe distances (2.74, 2.75 Å) are consistent with the existence of a single bond, being somewhat shorter than the corresponding "unexceptional" distances in $[CpMo(CO)_2]Fe(CO)_3(\mu_3\text{-Te})$ (2.84 Å)[48] and $[(C_5H_4Me)MoS_2\text{-}Fe(CO)_3]_2$ (2.95 Å)[49] and being similar in length to that found in $CpMoCo_2FeSAs(CO)_8$.[50]

The Mo−B bond lengths show variation within the cluster. The hydrogen-bridged linkages are of lengths comparable to those found in $(C_5H_4MeMo)_2B_5H_9$ (which average 2.32 Å[24]), although the bonds to B(1) at 2.36 Å are some 0.1 Å longer than those to B(5). This almost certainly reflects the positioning of the $Fe(CO)_3$ unit. Of the direct Mo−B linkages, those to B(2) and B(3) are unremarkable [2.15 and 2.16 Å, compared to 2.17 and 2.21 Å for comparable bonds in $(C_5H_4MeMo)_2\text{-}B_5H_9$[24]]. The bonds to B(4) are somewhat longer, however (2.30 and 2.31 Å), reflecting a weaker Mo−B interaction consistent with the large upfield ^{11}B NMR shift observed for this boron atom.

The comparison between **6** and the chromium compound **3** is of note not only from the point of view of probing unsaturation in the $(Cp^*Cr)_2B_4H_8$ precursor but also because of structural differences in the $Fe(CO)_3$ adducts themselves. **3** adopts a bicapped trigonal bipyramidal geometry in which the $Fe(CO)_3$ unit is face-capping and in which one pair of Cr−H−B hydrogens have become face- rather than edge-bridging. By contrast, in **6**, the $Fe(CO)_3$ unit occupies one of the vertexes of the octahedron with both capping atoms being borons. In some ways, this might be thought of as the more logical position for the iron fragment, since it allows the transition metal to attain a higher coordination number by occupying a vertex of higher connectivity. That the analogous situation does not occur in **3** (i.e., the $(Cp^*Cr)_2B_4H_8$ unit remains intact and the $Fe(CO)_3$ fragment is forced to take up a capping position) adds weight to the description of this compound as a coordination complex between an unsaturated metallaborane ligand and metal carbonyl.

The position of the boron resonance for B(4) calls for some comment. Although B(4) is directly bonded to both molybdenum atoms, as indeed it is in the starting material (**5**), its resonance is shifted some 60 ppm upfield from the corresponding signal of **5**. The only change in connectivity associated with B(4) is that it is now directly linked to three other borons, rather than two. B(4) is now considered to be occupying one of the apical vertexes of a bicapped octahedron. In B_5H_9, for example, the apical boron has a significantly more upfield chemical shift than the basal borons (by ca. 40 ppm), an effect attributed to the distribution of negative charge over the cluster framework.[51] It is conceivable, therefore, that the upfield shift of B(4) could be attributed to a similar effect. The other boron atoms in **6** show relatively small shifts from the corresponding positions in the starting material. Finally, it is interesting to note the large upfield shift for the Mo−*H*−B bridging hydrogens on going from **5** to **6** (δ_H −6.99 for **5**;[24] δ −15.5, −13.1 for **6**) despite the fact that both sets remain Mo−B edge-bridging.

The infrared spectrum of **6** shows three strong bands at 1994, 1947, and 1934 cm^{-1}, assigned to the CO stretching modes of the $Fe(CO)_3$ group. The positions of the bands are similar to those found in the IR spectrum of **3** (1978, 1916, and 1905 cm^{-1}),[15] being ca. 100 cm^{-1} lower than expected for a neutral ferraborane.[41−43] This in turn suggests a buildup of negative charge at the iron center in keeping with its occupation of an apical vertex of the bicapped octahedral structure. It should be noted, however, that the CO stretches for 1-$Fe(CO)_3B_4H_8$, in which the iron atom also occupies an apical vertex, are found at 2078 and 2018 cm^{-1}.[52] A Fenske−Hall molecular analysis was carried out on the molecule $(CpMo)_2B_5H_9Fe(CO)_3$ (**6′**) with coordinates based on the crystal structure of **6** in order to investigate the charge distribution in the cluster. These revealed a charge on the iron center similar to that found in **3** and positive charges on the molybdenum centers greater than those for the parent molybdaborane **5**. The results are consistent with the transfer of electronic charge to the iron center implied by the infrared frequencies.

Attempts to prepare the chromium analogue of **6**, $(Cp^*Cr)_2\text{-}B_5H_9Fe(CO)_3$, focused on two possible routes, viz. (i) the corresponding reaction of $(Cp^*Cr)_2B_5H_9$ (**2**) with $Fe_2(CO)_9$ and (ii) reaction of $(Cp^*Cr)_2B_4H_8Fe(CO)_3$ (**3**) with BH_3·thf. Route i yielded no discernible reaction, the amount of **2** remaining virtually unchanged over a reaction period of several weeks at 50 °C. The reaction of **3** with BH_3·thf did lead to consumption of the starting material **3**, although the only metallaborane product observed by ^{11}B NMR was **2**. Presumably, reaction of **3** with BH_3·thf proceeds predominantly via exchange of the isolobal BH and $Fe(CO)_3$ fragments with little tendency toward cluster expansion. The resistance of the bicapped trigonal bipyramidal chromium clusters **2** and **3** to expansion/rearrangement is in marked contrast to the ready conversion of the molybdenum species **5** to **6**.

Molecular Orbital Calculations. Fenske−Hall molecular orbital calculations were carried out in order to determine the electronic factors underlying (i) why the unsaturated species **1** is stable despite having two fewer electrons than required by the Wade−Mingos rules, (ii) why the saturated species **2**−**4** all show similar shortening of the Cr−Cr bond and lengthening of Cr−B linkages compared to the unsaturated species **1**, (iii) the nature of the metal−ligand interaction for the metal carbonyl

(48) Bogan, L. E.; Rauchfuss, T. B.; Rheingold, A. L. *J. Am. Chem. Soc.* **1985**, *107*, 3843.
(49) Cowans, B.; Noordik, J.; Rakowski Dubois, M. *Organometallics* **1983**, *2*, 931.
(50) Richter, F.; Vahrenkamp, H. *Organometallics* **1982**, *1*, 756.
(51) Odom, J. D.; Ellis, P. D.; Walsh, H. C. *J. Am. Chem. Soc.* **1971**, *93*, 3529.
(52) Greenwood, N. N.; Savory, C. G.; Grimes, R. N.; Sneddon, L. G.; Davison, A.; Wreford, S. S. *Chem. Commun.* **1974**, 718.

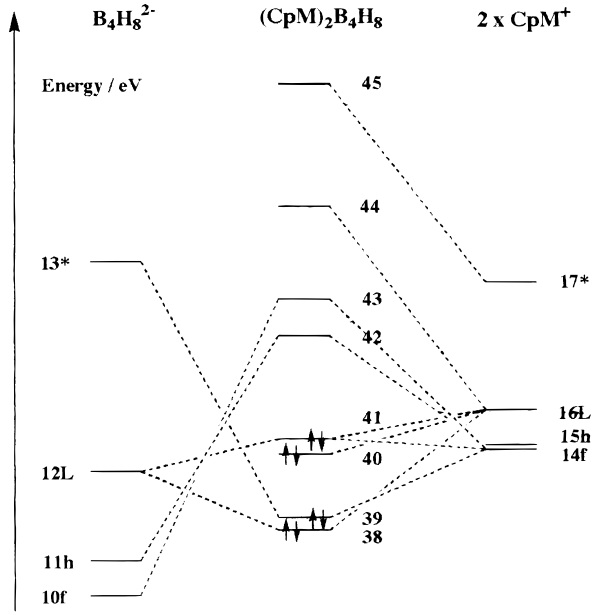

Figure 5. Molecular orbital scheme for $(CpM)_2B_4H_8$ [M = Cr (**1′**) or Mo (**7′**)].

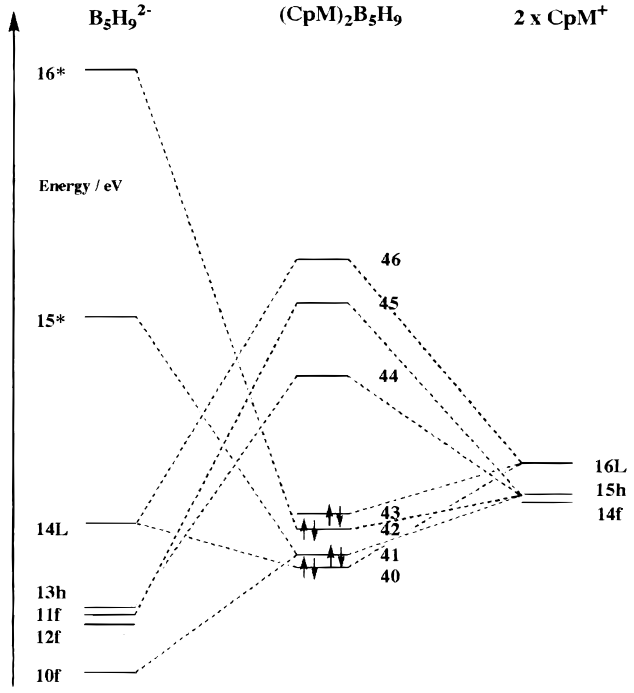

Figure 6. Molecular orbital scheme for $(CpM)_2B_5H_9$ [M = Cr (**2′**) or Mo (**5′**)].

species **3** and **4**, and (iv) differences in reactivity between the chromium and molybdenum systems. Molecular orbital schemes calculated for the $(CpM)_2B_4H_8$ and $(CpM)_2B_5H_9$ systems are reproduced in Figures 5 and 6, respectively. Molecular orbital energies are listed in Tables 9 and 10, respectively.

(i) Variation of the Borane Fragment. MO calculations were carried out for both B_4 and B_5 systems in order to determine the electronic factors underlying the stability of the unsaturated cluster **1** and the origins of the consistent geometric changes between **1** and saturated clusters such as **2**. The cluster $(Cp^*Cr)_2B_4H_8$ is thought of as being electronically unsaturated, having too few electrons (five sep's) to support the observed bicapped tetrahedral geometry.[12] This has been rationalized in terms of small but significant geometric changes (Cr−Cr lengthening, Cr−B shortening, B−B−B narrowing) which relative to a saturated derivative [such as $(Cp^*Cr)_2B_4H_8Fe(CO)_3$, **3**] cause the LUMO to move to higher energy and so stabilize the electron-deficient species.[16] $(Cp^*Cr)_2B_5H_9$, on the other hand, is saturated, having six sep's and a bicapped trigonal bipyramidal geometry. Relative to those of the B_4 derivative, the Cr−Cr distance is shorter (2.62 Å as opposed to 2.88 Å) and the average Cr−B distance longer (2.15 Å versus 2.07 Å).

Table 9. Molecular Orbital Energies for $(CpM)_2B_4H_8$ Species [M = Cr (**1′**) or Mo (**7′**)]

		energy (eV)	
fragment	mol orbital	Cr (**1′**)	Mo (**7′**)
CpM^+	16	−10.08	−8.34
	15	−11.10	−9.78
	14	−11.16	−10.48
$(CpM)_2B_4H_8$	45	−1.17	5.06
	44	−5.76	0.07
	43	−7.55	−5.26
	42 (LUMO)	−8.43	−6.54
	41 (HOMO)	−10.83	−10.17
	40	−11.12	−10.46
	39	−13.36	−13.58
	38	−13.89	−14.12

Table 10. Molecular Orbital Energies for $(CpM)_2B_5H_9$ Species [M = Cr (**2′**) or Mo (**5′**)]

		energy (eV)	
fragment	mol orbital	Cr (**2′**)	Mo (**5′**)
CpM^+	16	−10.03	−9.47
	15	−11.62	−10.88
	14	−11.68	−10.92
$(CpM)_2B_5H_9$	46	−3.87	0.07
	45	−6.33	−4.76
	44 (LUMO)	−7.97	−6.20
	43 (HOMO)	−12.54	−11.92
	42	−12.87	−12.75
	41	−13.35	−13.18
	40	−13.94	−13.96

A shorter (and by implication stronger) Cr−Cr bond is consistent with the much larger splitting between bonding and antibonding Cr−Cr $\sigma(d_{z^2})$ MOs found for **2′** (5.36 eV for **1′**, 8.57 eV for **2′**) and with the calculated Cr−Cr Mulliken overlap populations (0.06 for **1′**, 0.12 for **2′**). On the other hand, the longer Cr−B distances for **2′** are consistent with a weaker interaction between $(CpCr)_2$ and borane fragments, which is also reflected in the lower Mulliken overlap populations (0.21 for **1′**, 0.15 for **2′**). A stronger Cr−B interaction for the B_4 species is also consistent with a better energy match between the relevant $CpCr^+$ fragment orbitals and those of $B_4H_8^{2-}$ (orbitals 10−13) than is the case with $B_5H_9^{2-}$ (orbitals 9−15). In the B_5 case, many of the boron fragment orbitals involved in bonding lie deeper in energy and therefore interact less with the metal-based orbitals.

It is interesting to note that the characters of the HOMO and SHOMO are reversed on going from **1′** to **2′**. In **1′**, the HOMO (41) is primarily a Cr−Cr $\delta^*(d_{x^2-y^2})$ antibonding MO with essentially nonbonding Cr−B character, whereas the SHOMO (40) is mainly a Cr−Cr $\sigma(d_{z^2})$ bonding MO; the reverse is true for **2′**. The energy of the Cr−Cr $\sigma(d_{z^2})$ bonding MO falls slightly on going from the B_4 to the B_5 species (−11.12 eV for **1′**, −12.54 eV for **2′**), reflecting the stronger Cr−Cr bond, but the change of orbital ordering is largely due to the much larger fall in energy of the Cr−Cr $\delta^*(d_{x^2-y^2})$ antibonding MO (−10.83 for **1′**, −12.87 for **2′**). The origin of this energy difference is set out in Figure 7 and lies in fact that the Cr−B interaction is

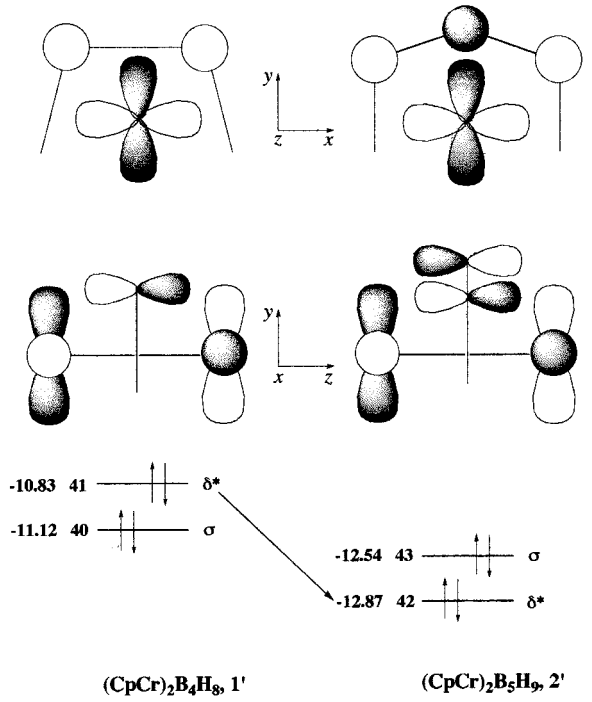

Figure 7. Stabilization of the Cr−Cr δ* MO for $(CpCr)_2B_5H_9$ (**2′**) vs $(CpCr)_2B_4H_8$ (**1′**). The M−B interaction changes from essentially nonbonding to bonding by overlap with the p_z orbital of the extra unique boron.

bonding in the B_5 case but essentially nonbonding in the B_4 compound. The major contribution to this MO comes from overlap of a $\pi(p_z)$-type borane fragment orbital with the δ*-type metal fragment orbitals. In the B_4 case, this is essentially nonbonding, but for the B_5 species, the presence of the p_z orbital on the extra unique boron, B(3), gives rise to a favorable bonding overlap with the metal-based orbitals. This additional bonding effect is accentuated by the shorter Cr−Cr distance for **2′**. Consequently, relative to the corresponding orbital in **1′** (41), MO 42 (for **2′**) falls in energy such that it lies below the Cr−Cr $\sigma(d_{z^2})$ MO (43).

It is of note that, for both molybdenum and chromium compounds, the HOMO/LUMO gap is significantly larger for the B_5 compound than for its B_4 counterpart; this observation can also be explained in terms of two of the factors mentioned above. For the chromium compounds, **1′** and **2′**, the LUMO differs little in energy (−8.43 eV for **1′**, −7.97 eV for **2′**) and the larger HOMO/LUMO gap is principally due to the much lower energies of the HOMO and SHOMO in the B_5 case. This in turn is due to the more favorable Cr−Cr (for MO 43—HOMO) and Cr−B (for MO 42—SHOMO) bonding interactions compared to their counterparts in the B_4 eigenvalue spectrum.

(ii) Variation of Metal. Calculations carried out on the molybdenum metallaboranes were expected to reveal changes consistent with the presence of the heavier transition metal and, it was hoped, might shed some light on the higher reactivity of the molybdenum species compared to their chromium counterparts (i.e., nonisolation of the Mo_2B_4 cluster analogous to **1** and the ready cluster expansion of **5** to the bicapped octahedral species **6**). Qualitatively the ordering of MOs for both $(CpM)_2B_4H_8$ and $(CpM)_2B_5H_9$ species varies little as the metal changes from chromium to molybdenum. For each molecule, the HOMO/LUMO gap is significantly greater (by ca. 2.3 eV) in the molybdenum case, in part reflecting the stronger M−M interaction for the 4d metal over the 3d. As expected, for both B_4 and B_5 species, the Mulliken overlap populations for the M−M unit are significantly higher in the molybdenum case (0.06 and 0.09 for **1′** and **7′**, respectively; 0.12 and 0.14 for **2′** and **5′**, respectively).

In the case of the B_5 species, the positions of the bonding MOs (40−43) change little between chromium and molybdenum and the much larger HOMO/LUMO gap derives from the significantly higher energies of the unoccupied orbitals (44−46) in the molybdenum case. MO 46 is primarily a M−M antibonding σ*(d_{z^2}) orbital and would be expected to be at higher energy for molybdenum, reflecting the stronger metal−metal interaction. MOs 44 and 45 are chiefly M−B antibonding in character and lie ca. 1.6 eV higher in the molybdenum case; additionally, these orbitals have significantly greater contribution from $B_5H_9^{2-}$-based fragment orbitals in the molybdenum compound than in the chromium counterpart. These factors tend to suggest a stronger M−B interaction in the molybdenum case, an assertion given further weight by the calculated M−B Mulliken overlap populations (0.15 for **2′**, 0.22 for **5′**). Furthermore, the M−H overlap populations are also larger in the molybdenum case (0.11 for **2′**, 0.15 for **5′**), the overall conclusion being that the interaction between $(CpM)_2$ and B_5H_9 fragments is stronger in the molybdenum compound. A very similar situation occurs for the $(CpM)_2B_4H_8$ species, where the HOMO/LUMO gap is again noticeably higher in the molybdenum case. Here too this is chiefly due to the considerably higher energies of the lowest three unoccupied MOs (42−44) for molybdenum.

(iii) Fragment Analysis of $(CpCr)_2B_5H_9$. In a manner similar to the fragment analysis carried out for $(CpCr)_2B_4H_8Fe(CO)_3$, **3′**,[15,16] a treatment of the MO eigenvectors of **2′** was carried out in order to determine the nature of the interaction between BH and distorted $(CpCr)_2B_4H_8$ fragments. There are significant changes in the MO eigenvalue spectrum on going from **1′** to **2′**, and the primary purpose of the fragment analysis was to determine which changes are due principally to distortion of the $(CpCr)_2B_4H_8$ unit [compression along the Cr−Cr axis and opening of the B_4 unit between B(2) and B(3)] and which are due to the presence of the extra unique boron. The results are outlined schematically in Figure 8.

Clearly, distortion of the $(CpCr)_2B_4H_8$ fragment is much greater than occurs in $(CpCr)_2B_4H_8Fe(CO)_3$, **3′**, reflecting the fact that the extra BH unit in $(CpCr)_2B_5H_9$ is formally inserted between B(2) and B(3) whereas the $Fe(CO)_3$ fragment in **3′** is bound to the open face of the $(CpCr)_2B_4H_8$ unit.[15,16] The principal MO changes on going from **1′** to the distorted $(CpCr)_2B_4H_8$ fragment reflect changes in the Cr−Cr and B(2)−B(3) distances. MOs which are principally Cr−Cr bonding in nature fall in energy as a result of the shortened Cr−Cr distance. On the other hand, MOs featuring a significant B(2)−B(3) bonding interaction are raised in energy as the atoms are forced further apart.

Interaction of the distorted $(CpCr)_2B_4H_8$ fragment with the BH unit involves two principal points of contact, as shown by the lines on the correlation diagram (Figure 8). The HOMO and the LUMO of the distorted $(CpCr)_2B_4H_8$ fragment interact with the pair of degenerate unoccupied π-type orbitals of the BH unit (essentially the p_x and p_z orbitals of the boron atom). The nature of these interactions is shown in Figure 9. Overlap of the HOMO with the p orbital lying parallel to the *x* axis gives rise to MOs 35 (bonding—occupied) and 45 (antibonding—unoccupied), whereas interaction of the LUMO with the π_z type BH fragment orbital gives rise to MOs 42 and 46. With regard to MO 42 (for **2′**), we have essentially come to the conclusion which was touched on earlier, namely that the stabilization of

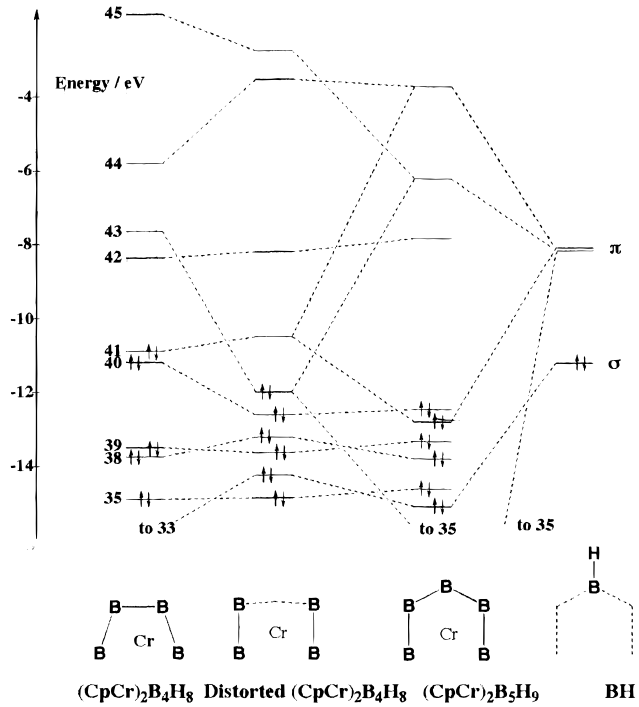

Figure 8. Molecular orbital scheme for $(CpCr)_2B_5H_9$ (**2′**) based on BH and distorted $(CpCr)_2B_4H_8$ fragments.

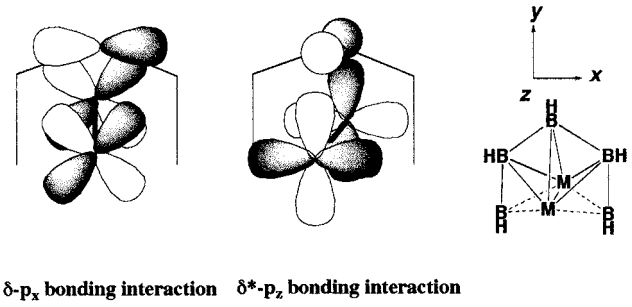

Figure 9. Principal interactions between BH and distorted $(CpCr)_2B_4H_8$ fragments for $(CpCr)_2B_5H_9$ (**2′**).

this orbital compared to its counterpart in **1′** (MO 41) is almost entirely due to the extra Cr−B bonding provided by the unique boron B(3). Furthermore, it is of note that compared to the distorted $(CpCr)_2B_4H_8$ fragment (or to the undistorted molecule **1′**) there is one extra bonding MO in **3′** to accommodate the increase in sep's from 5 to 6. In **1′**, MO 41 was filled and MO 43 empty, but the combination of geometric changes and interaction with the empty π orbitals of the extra BH unit contrive to lower the energies of these orbitals, such that their counterparts in **2′** are much lower in energy and both are occupied.

(iv) Fenske−Hall Calculations for $(CpCr)_2B_4H_7Co(CO)_3$ (4′). MO calculations were carried out for **4′** in order to determine the nature of the interactions between the $Co(CO)_3$ fragment and the $(CpCr)_2B_4H_7$ cluster ligand. This analysis would hopefully add weight to the description of both **3′** and **4′** as coordination complexes and help to explain structural differences with the isoelectronic cluster **2** (i.e., the positions of the bridging hydrogen atoms). The Fenske−Hall analysis of $(CpCr)_2B_4H_7Co(CO)_3$ has been examined in terms of odd-electron $(CpCr)_2B_4H_7$ and $Co(CO)_3$ fragments. The analysis is very similar to that for the corresponding iron carbonyl species, $(CpCr)_2B_4H_8Fe(CO)_3$ (**3′**).[16] The principal changes between the ground state $(CpCr)_2B_4H_8$ molecule and the $(CpCr)_2B_4H_7$ fragment in **4′** reflect the shorter Cr−Cr distance (2.694 vs 2.88 Å) and longer mean Cr−B distance (2.15 vs 2.06 Å) (again similar to the case of the iron complex) and involve sharp increases in energy for those fragment orbitals which are Cr−Cr antibonding and Cr−B bonding. This is particularly marked for the $\delta^*(d_{x^2-y^2})$ fragment orbital (41) such that the ordering of orbitals in this region is altered.

The principal interactions between the two fragments then involve bonding and antibonding combinations of the two orbitals of e symmetry [for a C_{3v} $Co(CO)_3$ fragment], 19 and 20, with the $\delta(d_{x^2-y^2})$ and $\delta^*(d_{x^2-y^2})$ orbitals of the chromium fragment (41 and 42). This gives rise to the stabilized bonding orbitals 59 and 60 and the higher energy unoccupied MOs 62 and 64. In addition, the empty σ orbital of the $Co(CO)_3$ fragment interacts with a lower lying, filled B−H−Cr orbital generating a bonding, donor−acceptor interaction with the cobalt center. This interaction causes the hydrogen atom to become Cr−B−Co face-bridging, rather than edge-bridging as seen in both the isoelectronic species **2** and the starting cluster **1**.

Discussion

The structural response of a Lewis acid to the addition of a base constitutes a probe of the electronic structure of the acid. Likewise, one can view the structural response of a cluster to the addition of a two-electron cluster fragment as a probe of the cluster electronic structure. Recently, we reported that the addition of a two-electron $Fe(CO)_3$ fragment to $(Cp^*Cr)_2B_4H_8$ (**1**) resulted in only minor geometric changes to the latter.[15] **1** behaves as a complex metallaborane ligand in satisfying the electronic requirements of the iron center, while in turn accepting two electrons. We argued that the null geometric response of **1** is consistent with the delocalized deficiency of two cluster bonding electrons suggested on the basis of electron count (five pairs), MO calculations, and reactivity.[12,15] Addition of the isolobal BH fragment to **1** results in complete insertion to form a product with a cluster structure based on a bicapped trigonal bipyramid, **2** in Scheme 1. As the tetrahedron and trigonal bipyramid (capped tetrahedron) have the same electron count (six sep's) it could be argued that the null geometric change observed for the addition of $Fe(CO)_3$ to **1** says nothing concerning the electronic structure of **1**.

We noted that the hydrogen-bridged faces of the Cr_2B_4 species **1** and the M_2B_5 clusters **2** (M = Cr) and **5** (M = Mo) are very similar in geometry and wondered if either **2** or **5** could act as a ligand toward an $Fe(CO)_3$ fragment in like manner. If so, it would provide a test of the above arguments. Two limiting scenarios are possible. In the first, **2** or **5** might simply chelate the $Fe(CO)_3$ fragment without accepting a pair of electrons from the iron center and retain its basic geometry on coordination. This would imply that the null geometry change in **1** described above has a similar explanation and has no bearing on its unsaturation. On the other hand, if **2** or **5** reacted with $Fe_2(CO)_9$ accepting a pair of electrons, then, being saturated, it should rearrange to produce a cluster based on a bicapped octahedron. The observed retention of cluster geometry in **1** as geometric evidence of its electronic unsaturation would now be corroborated.

We have examined the reaction of the Mo_2B_5 species **5** with $Fe_2(CO)_9$ and the result is unambiguous. Addition of an $Fe_2(CO)_9$ fragment to **2** results in the unmistakable cluster structure change predicted by the Wade−Mingos rules.[47] Thus the electronic unsaturation in **1** is corroborated.

The saturated six-sep clusters **2**−**4** all display similar structural changes when compared to the unsaturated cluster **1** from which they are derived (most noticeably shortening of the

Cr−Cr bond by up to 10%, lengthening of Cr−B linkages, and opening of the B−B−B angles). A recent MO comparison of the clusters **1** and **3** and the six-sep cluster $(Cp^*Cr)_2B_4H_6(CO)_2$ concluded that the properties of the $(Cp^*Cr)_2$ unit are such that the "t_{2g}" metal orbitals not only have energies appropriate for cluster bonding but are also easily perturbed, thereby effectively changing the metal fragment contribution to cluster bonding.[16] As such, small changes in cluster geometry brought about by compression along the Cr−Cr axis and elongation perpendicular to it cause an unfilled MO to be lowered in energy such that it can now be occupied and six sep's can be accommodated for **3** and $(Cp^*Cr)_2B_4H_6(CO)_2$ without any gross structural change (e.g., bond formation or breakage) from the five-sep cluster **1**. That similar geometric changes are also observed for the clusters **2** and **4** adds further weight to these arguments in which the cluster geometry is effectively invariant to the Wade electron count.[47] Alternatively, one can view the stabilization of the unsaturated species **1** as being derived from elevation of the LUMO into the region of high-energy unoccupied orbitals such that it is then energetically unprofitable to occupy this MO and **1** is stable despite two electrons fewer than in the saturated species **2**−**4**. The LUMO for **1** is Cr−Cr bonding and Cr−B antibonding, so lengthening of the Cr−Cr bond and compression of the Cr−B linkages bring about the necessary elevation of the LUMO.

Reaction of the group 6 metallaboranes with sources of BH and $M(CO)_3$ fragments constitute high-yield controlled cluster expansion reactions and useful routes to targetted mixed-metal clusters. Addition of a BH fragment to **1** generates the Cr_2B_5 species **2**, and although attempts to ascertain the reaction mechanism by using "labeled" BCl or BR fragments were unsuccessful, an attractive possibility involves initial coordination of the BH fragment to the open face of the molecule in a manner akin to that seen for the isolobal $Fe(CO)_3$ fragment in **3**, followed by migration of bridging hydrogens to the Cr−B bonds now constituting the open face of the molecule. Initial coordination of the BH fragment would involve the formation of two Cr−B linkages and two BH→B donor−acceptor linkages, a process likely to imply a lower activation barrier than direct insertion into one of the B−B bonds. Interestingly, the idea of the open face of the cluster as an initial site of reactivity might explain why both Cr_2B_4 and Mo_2B_5 clusters are reactive toward cluster expansion reactions with $Fe(CO)_3$, yet the Cr_2B_5 species **2** is not (**2** has a somewhat smaller open face than **1** or **5**, as defined by M−M and B···B linkages). On the other hand, the Cr_2B_4Fe cluster **3** reacts with BH_3·thf to give the substitution product **2**, rather than the cluster expansion product $(Cp^*Cr)_2B_5H_9Fe(CO)_3$, and it may simply be that in the chromium case the smaller size of chromium vs molybdenum prevents the buildup of an octahedral cluster around the $(Cp^*M)_2$ unit on steric grounds.

The mixed-metal species **3** and **4** represent unusual examples of clusters acting as ligands for a transition metal center. Coordination through donor−acceptor linkages is not uncommon for neutral or anionic borane fragments (e.g., BH_4^-, $B_3H_8^-$, or B_6H_{10}), although for metallaborane clusters this behavior is extremely rare. Given the response of the saturated cluster **5** to addition of an $Fe(CO)_3$ fragment (i.e., cluster rearrangement in line with the Wade−Mingos rules), it seems likely that the propensity of **1** to act as a ligand for transition metal centers (without gross structural changes) is intrinsically linked to its unsaturation. As such, it will be interesting to investigate the ability of other recently synthesized unsaturated metallaboranes [e.g., $(Cp^*MoCl)_2B_3H_7$[13] or $Cp^*TaCl_2B_4H_8$[14]] to act as similar ligands.

Acknowledgment. The support of the National Science Foundation is gratefully acknowledged. S.A. also thanks the J. William Fulbright Scholarship Board for the award of a research scholarship.

Supporting Information Available: Tables of crystal data, positional and equivalent isotropic thermal parameters, bond distances and angles, and general displacement parameter expressions for compounds **2**−**4** and **6**, along with a Fenske−Hall molecular orbital scheme for **4′** (68 pages). Crystallographic files, in CIF format, are available on the Internet only. Ordering and access information is given on any current masthead page.

IC971251K